Journal of
Composites Science

MDPI

Article

Comprehensive Analysis of Wear, Friction, and Thermal Resistance in PVDF/Nanoclay Composites Using Taguchi Methodology for Enhanced Tribological Performance

Pavan Hiremath [1], R. C. Shivamurthy [1,*], Giridhar B. Kamath [2,*] and Nithesh Naik [1]

[1] Department of Mechanical and Industrial Engineering, Manipal Institute of Technology, Manipal Academy of Higher Education, Manipal 576104, Karnataka, India; pavan.hiremath@manipal.edu (P.H.); nithesh.naik@manipal.edu (N.N.)
[2] Department of Humanities and Management, Manipal Institute of Technology, Manipal Academy of Higher Education, Manipal 576104, Karnataka, India
* Correspondence: shivamurthy.rc@manipal.edu (R.C.S.); giridhar.kamath@manipal.edu (G.B.K.)

Abstract: This study discusses the tribological characteristics of Polyvinylidene Fluoride (PVDF)/nanoclay composites, focusing on the effects of nanoclay content (0, 1, 2 and 3 wt.%), load, sliding speed, and sliding distance on the wear rate, friction coefficient, specific wear rate, and temperature. A Taguchi Design of Experiments technique was applied to optimize and assess these aspects. The results demonstrated that nanoclay addition considerably improved the wear resistance and frictional stability of the PVDF composites. Specifically, a nanoclay concentration of 3 wt.% gave the lowest wear rate (0.05 mg/m) with a 10 N load and 100 m sliding distance, lowering wear by roughly 23% compared to unreinforced PVDF. The friction coefficient was similarly lowered by 12% with 3 wt.% nanoclay, reaching a value of 0.38 at the highest load of 40 N. Interaction effects demonstrate that load and sliding distance are key elements impacting wear performance, with large loads and long distances virtually tripling the wear rate. ANOVA results quantify nanoclay's contribution to a wear rate reduction of 51.29%, whereas load and sliding distance contributed 22.47% and 16.98%, respectively. Temperature increases due to frictional heating reached 10 °C under rigorous test conditions, although nanoclay treatment decreased this increase by an average of 15%. Characterization by XRD and FTIR verified the nanoclay dispersion inside the PVDF matrix, whereas the SEM images demonstrated smoother surfaces and fewer wear tracks in the nanoclay-reinforced samples. These findings illustrate the efficiency of nanoclay in increasing the wear resistance of PVDF, making these composites appropriate for high-performance applications. This research provides useful insights into enhancing PVDF/nanoclay composites, with possible uses in situations that demand endurance and thermal stability.

Keywords: PVDF/nanoclay composites; wear resistance; friction coefficient; Taguchi analysis; tribological properties

check for updates

Academic Editor: Giuseppe Cavallaro

Received: 5 December 2024
Revised: 31 December 2024
Accepted: 4 January 2025
Published: 14 January 2025

Citation: Hiremath, P.; Shivamurthy, R.C.; Kamath, G.B.; Naik, N. Comprehensive Analysis of Wear, Friction, and Thermal Resistance in PVDF/Nanoclay Composites Using Taguchi Methodology for Enhanced Tribological Performance. *J. Compos. Sci.* **2025**, *9*, 37. https://doi.org/10.3390/jcs9010037

Copyright: © 2025 by the authors. Licensee MDPI, Basel, Switzerland. This article is an open access article distributed under the terms and conditions of the Creative Commons Attribution (CC BY) license (https://creativecommons.org/licenses/by/4.0/).

1. Introduction

Polymer composites offer a high strength-to-weight ratio, excellent corrosion resistance, and thermal stability, making them ideal for aerospace, automotive, and electronic applications. Their properties can be tailored through reinforcements, enabling versatility for various industries. However, challenges include high manufacturing costs, complex processing requirements, and difficulties in recycling due to their heterogeneous nature.

Addressing these limitations is critical for advancing their use in sustainable and high-performance applications [1].

Polymer nanocomposites are formed by the integration of nanoparticles into a polymer matrix, provided the nanoparticles are dispersed and distributed at the nanoscale throughout the matrix. These nanocomposites exhibit superior performance characteristics compared to those of conventional polymers. This enhancement in the characteristics and properties is primarily attributed to the minimal nanoparticle loading in the polymer matrix, as these nanoparticles tend to disperse more effectively within the matrix [2]. However, the inclusion of macro fillers can introduce certain drawbacks to the resultant composite material, such as increased brittleness owing to the limited interaction between the polymer and filler [3]. Nanofillers like nanoclay, carbon nanotubes, and other nanoparticles serve as key reinforcements in polymer nanocomposites due to their multifunctional and improved properties. The incorporation of these nanofillers has resulted in better dispersion within the polymer matrix, thereby enhancing the properties of the polymer [4].

Polymer composites are used in mechanical engineering for frictional and structural materials owing to their low density, simple processing, strength, thermal stability, and wear resistance. They are essential for tribological applications in various industries, including electronics, aerospace, automotive, and biomechanics. The polymer characteristics improved when nanoparticles were added, broadening their applicability. The tribological characteristics of polymers, for instance, are enhanced by the addition of fillers such as reinforcing fibers [5].

In terms of chemical and thermal stability, fluoropolymers such as Polyvinylidene Fluoride (PVDF) outperform hydrocarbon polymers. PVDF is employed in sectors such as paper and pulp, chemical processing, and high-temperature applications because of its solvent resistance, UV exposure tolerance, and thermal oxidative degradation durability. Owing to its piezoelectric and pyroelectric capabilities, it is used in water purification, lithium batteries, sensors, and electromechanical and electroacoustic transducers [6,7].

The nonpolar and polar phases of PVDF—a semi-crystalline polymer with four phases—have been extensively studied. The polar phase demonstrates dielectric, high permittivity, ferroelectric, piezoelectric, and ferroelectric characteristics. A filler material was added to PVDF to improve its morphology, structure, and functional characteristics [8]. Different functional characteristics are induced in PVDF by ionic chemicals, carbon black, carbon nanotubes, and two-dimensional materials, such as graphene. The electroactive phase is induced by methods such as melt crystallization, high-voltage poling, and mechanical processing [9].

High-strength carbon fibers based on fluorinated polyacrylonitrile were used by Bismarck and Schulz [10] to strengthen PVDF composites, and they found that friction decreased with the fluorination level of the fiber fluorinates. To improve the tribological properties of PVDF, several fillers, including graphene oxide, carbon black, carbon fiber, and nanoclay, have been used. The tribological characteristics of a PVDF/ultrahigh molecular weight polyethylene (UHMWPE) mixture with different quantities of carbon black and irradiation were studied by Li et al. [11]. They observed that optimized carbon black concentrations and irradiation dosages resulted in less wear, more scratch resistance, and less friction.

Afonso et al. [12] described the wear and mechanical characteristics of PVDF/PMMA blends based on the phase morphology, with the exception of the basic additive rule. By creating a PVDF/reduced graphene oxide nanocomposite via melt blending, Hintermueller and Prakash [13] significantly improved its flexural modulus, tensile modulus, flexural strength, tensile strength, and thermal stability. Paul et al. [14] looked at the tribological characteristics of PVDF/nanoclay composites with various nanoclay contents and found

that the composite containing 2 wt.% nanoclay had improved characteristics. After analyzing the tribological characteristics of thin films made of functionalized graphene oxide and PVDF, Thangavel et al. [15] discovered that they were stable even after 120 cycles of reciprocating motion under a 10 mN load. Polymer-layered silicate nanocomposites are essential components of composite technology.

Abu-Zurayk et al. [16] created PVDF/nanoclay nanocomposites with various organic modifiers and noticed improved mechanical strength and abrasion resistance. Hosseini et al. [17] showed a significant improvement in the storage modulus of PVDF/clay nanocomposites prepared using the melt intercalation technique. Additionally, it has been discovered that nanoclay significantly enhances the tribological characteristics of polyesters and polyamides.

In this study, solution-processed PVDF/nanoclay composites with different nanoclay contents were fabricated. This study focused specifically on investigating the tribological properties of these composites. Various analytical techniques have been employed to examine the structure, morphology, and thermal characteristics of the composites. However, the primary emphasis was on evaluating the friction and tribological properties of the PVDF/nanoclay composites along with the mechanical characteristics that were studied.

Response surface analysis was employed to analyze the relationship between the nanoclay content and tribological properties. This statistical technique allows one to model and optimize the tribological behavior of composites by studying the influence of varying the nanoclay content [18,19]. Predictive models were generated by systematically altering the nanoclay content and observing the resulting changes in the tribological characteristics. These models helped uncover the optimal nanoclay content for achieving enhanced tribological performance in PVDF/nanoclay composites. By utilizing response surface analysis, this study offers a quantitative understanding of how nanoclay content affects the tribological properties of PVDF composites. This approach provides valuable insights into the design and optimization of PVDF/nanoclay composites for applications requiring improved frictional performance and wear resistance.

Additionally, the incorporation of nanoclay into the PVDF matrix enhances its mechanical and thermal stability by reinforcing the polymer's microstructure. The lamellar structure of nanoclay acts as a barrier to polymer chain movement, thereby reducing material deformation under stress. This interaction not only improves wear resistance but also ensures consistent frictional behavior, even under high-stress conditions. The synergistic effect of nanoclay's intrinsic properties and its dispersion within the PVDF matrix further highlights its potential in addressing the limitations of conventional PVDF for demanding applications [20,21].

Improving the tribological performance of polymers like PVDF is a significant problem in applications requiring endurance and heat stability, such as in the aerospace, automotive, and biomedical sectors. Conventional PVDF frequently demonstrates constraints, including elevated wear rates and frictional instability under challenging situations. Nanoclay, characterized by its distinctive lamellar structure, elevated aspect ratio, and thermal stability, offers a viable answer to these issues. This study posits that the integration of nanoclay into PVDF will markedly improve its tribological characteristics by decreasing wear rates, frictional forces, and thermal deterioration.

This study provides a detailed analysis of the tribological and thermal performance of PVDF/nanoclay composites, emphasizing dynamic wear behavior and optimizing properties using response surface methodology. By integrating structural validation and statistical modeling, this work offers novel insights into designing polymer nanocomposites for applications requiring enhanced wear resistance and thermal stability, distinguishing it from similar studies in the field.

2. Materials and Methods

2.1. Polymer and Nanoclay

The PVDF polymer with an average molecular weight of 2.65 × 10^5 g/mol used in this study was procured from JJ Polymers, Maharashtra, India. Organically modified nanoclay (Cloisite 30B) with a density of 1.92 g/cc and surface modification by quaternary ammonium salts (containing methyl, tallow, and bis (2-hydroxyethyl) functionalities) was supplied by nanochemazone.com. The nanoclay had a reported purity of 99% and was used as received. N, N- DMF, used as the solvent for both PVDF and nanoclay dispersion, was obtained from Alpha Chemistry, Maharashtra, India, with a purity of 99.9%. Table 1 lists the properties of the nanoclay used in this study.

Table 1. Comprehensive properties of nanoclay used in PVDF composites.

Property	Details
Type	Organically modified with quaternary ammonium compounds
Cation Exchange Capacity (CEC)	95 meq/100 g
Particle Size	<250 nm
Aspect Ratio	High
Specific Surface Area	~750 m^2/g
Thermal Stability	Up to 350 °C
Density	1.7 g/cm^3
Color	Off-white to pale yellow
Moisture Content	<2%
pH in Water Suspension	7–8
Dispersion Medium	Compatible with DMF and acetone
Functionality	Enhanced compatibility, improved dispersion, and mechanical reinforcement

2.2. Nanocomposite Preparation

Nanocomposites composed of PVDF and organically altered nanoclay were synthesized using a solution-based approach. Various nanoclay concentrations were employed in the preparation of these nanocomposites (0, 1, 2, and 3 wt.% of nanoclay relative to the weight percentage of polymer). In this process, PVDF was initially dissolved in DMF at 50 °C, and the nanoclay was dispersed distinctly via sonication. Subsequently, the polymer and nanoclay solutions were combined by stirring and additional sonication to ensure thorough dispersion. The solvent was then removed by transferring the mixture into a Petri dish and allowing it to dry overnight at 50 °C in a zero-pressure oven. PVDF was dissolved in DMF and dried in an oven for solvent exclusion. Later, the specimens were prepared in a wooden mold with the required diameter (8 mm) based on the ASTM G99 standard for the pin-on-disc wear test. Figure 1 presents a pictorial representation of the methodology employed in this study.

2.3. Material Characterizations

The exfoliation of nanoparticles and structural changes in the nanocomposites were analyzed by X-ray diffraction (XRD) using an XRDynamic 500 diffractometer (Anton Paar GmbH, Graz, Austria). XRD plots were obtained for the pristine polymer and its nanocomposite using Cu Kα radiation (λ = 0.1542 nm). The d-spacing, which represents the distance between the clay platelets, was calculated using Bragg's formula.

Fourier transform infrared spectroscopy (FTIR) was performed using a Bruker Tensor II FTIR Spectrometer (Bruker Corporation, Billerica, MA, USA) in the 600–4500 cm^{-1} range with a resolution of 4 cm^{-1} in the ATR mode. This technique allowed for the analysis of the molecular vibrations and functional groups present in the samples.

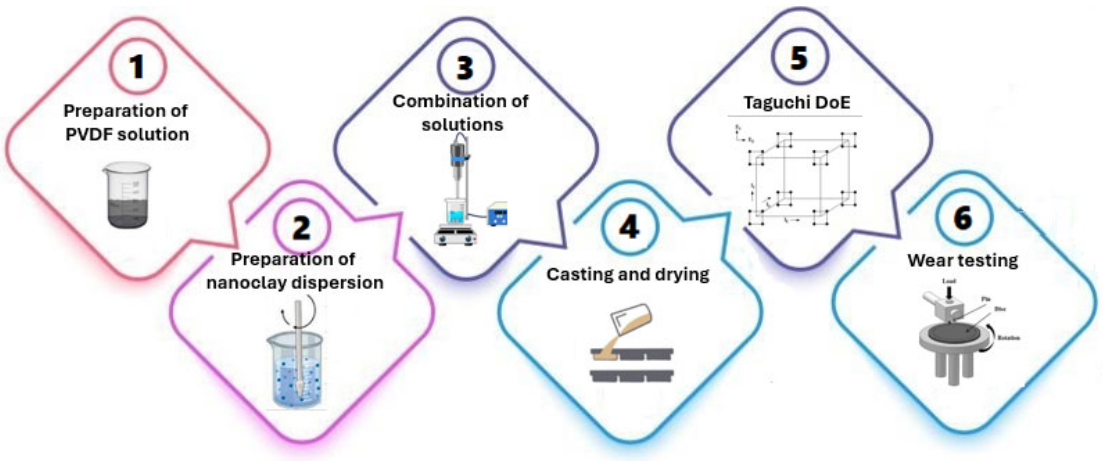


Figure 1. Preparation and testing of PVDF/nanoclay nanocomposites.

Wear testing of the PVDF/nanoclay composites was conducted using a pin-on-disc tribometer (Ducom Instruments, Bengaluru, India) in accordance with the ASTM G99 standards.The specimen, measuring 8 mm in diameter, underwent testing under loads ranging from 10 N to 40 N, sliding speeds of 0.5 to 2.0 m/s, and sliding lengths of 100 m to 400 m to assess the wear rate, friction coefficient, and specific wear rate [22]. The frictional force and temperature were measured in real time to determine the wear rate of the material volume loss.

This study analyses the influence of nanoclay concentration (0, 1, 2 and 3 wt.%), load (10, 20, 30 and 40 N), sliding speed (0.5, 1, 1.5 and 2 m/s) and sliding distance (100, 200, 300 and 400 m) on the tribological characteristics of PVDF/nanoclay composites. A Taguchi Design of Experiments was performed to systematically modify these parameters, allowing for the study of wear rate, friction coefficient, specific wear rate, and temperature rise. Statistical techniques, including ANOVA and interaction graphs, were applied to investigate the contributions and interactions of these factors. The following Taguchi DOE (Table 2) delineates the experimental setup and findings pertaining to the contributions to comprehending the influences on the wear performance under controlled tribological circumstances.

The counter body (disc) used in the pin-on-disc tests was made of hardened stainless steel with an initial surface roughness (Ra) of approximately 0.3 μm. The roughness of the contact surfaces of both the pin and the disc was measured before and after testing using a surface profilometer, following the ASTM G99 standard. The PVDF/nanoclay composite pins initially exhibited a roughness of 0.4 ± 0.05 μm, which increased to 0.7 ± 0.08 μm after testing. Similarly, the stainless-steel disc showed an increase in roughness from 0.3 ± 0.03 μm to 0.5 ± 0.06 μm after testing.

The results in Table 2 from the experiment on PVDF/nanoclay composites were studied using prediction models for the wear rate, friction coefficient, specific wear rate, and temperature rise. Input variables in the models include values of load (N), sliding speed (m/s), sliding distance (m), and nanoclay content (wt.%) for estimating the tribological behavior at different phases. This analysis examined the influence of each parameter on the results, with observed patterns compared to the theoretical models generated.

Table 2. Taguchi Design of Experiments (DOE) for wear testing of PVDF/nanoclay composites.

Nanoclay (wt.%)	Load (N)	Sliding Speed (m/s)	Sliding Distance (m)	Wear Rate (mg/m) ±SD	Friction Coefficient (μ) ± SD	Specific Wear Rate (mm^3/Nm)	Temperature Increase (°C)
0	10	0.5	100	0.06 ± 0.002	0.35 ± 0.01	1.2	5
0	20	1	200	0.08 ± 0.003	0.36 ± 0.02	1.3	7
0	30	1.5	300	0.09 ± 0.004	0.37 ± 0.02	1.4	8
0	40	2	400	0.10 ± 0.005	0.39 ± 0.03	1.5	10
1	10	1	300	0.07 ± 0.003	0.34 ± 0.02	1.1	6
1	20	0.5	400	0.08 ± 0.002	0.35 ± 0.01	1.2	7
1	30	2	100	0.06 ± 0.002	0.33 ± 0.01	1	6
1	40	1.5	200	0.09 ± 0.003	0.36 ± 0.02	1.3	8
2	10	1.5	400	0.07 ± 0.002	0.34 ± 0.01	1.1	7
2	20	2	300	0.08 ± 0.003	0.35 ± 0.02	1.2	8
2	30	0.5	200	0.09 ± 0.004	0.36 ± 0.02	1.3	7
2	40	1	100	0.07 ± 0.003	0.34 ± 0.01	1.1	6
3	10	2	200	0.05 ± 0.001	0.32 ± 0.01	0.9	6
3	20	1.5	100	0.06 ± 0.002	0.33 ± 0.01	1	7
3	30	1	400	0.07 ± 0.003	0.34 ± 0.01	1.1	8
3	40	0.5	300	0.08 ± 0.004	0.35 ± 0.02	1.2	9

2.3.1. Wear Rate and Specific Wear Rate

The wear rate (W) and specific wear rate (W_s) are calculated based on the following modified Archard's wear law in Equations (1) and (2), respectively:

$$W = k \cdot \frac{F^a \cdot v^b \cdot d}{H \cdot (1 + \alpha C)} \tag{1}$$

$$W_s = \frac{W}{F \cdot d} = \frac{k \cdot F^{a-1} \cdot v^b}{H \cdot (1 + \alpha C)} \tag{2}$$

where F is the load, v is the sliding speed, d is the sliding distance, H is the hardness of the composite, k is the wear coefficient specific to PVDF/nanoclay composites, C is the nanoclay content, and α is the reinforcement factor. As noticed in the table, the wear rate W increases with load (F) and sliding speed (v), which agrees with the model's dependency on F^a and v^b [23]. Increasing nanoclay content from 0% to 3% decreases the wear rate and specific wear rate across all test settings. This impact is described by the $(1 + \alpha C)$ equation, where nanoclay adds extra reinforcement, boosting the hardness and wear resistance of the composite. For instance, at 0% nanoclay, increasing the load from 10 N to 40 N (with matching increases in sliding speed and distance) raises the wear rate from 0.06 mg/m to 0.1 mg/m. However, with 3% nanoclay, the wear rate is lowered to a range of 0.05–0.08 mg/m across identical settings, confirming nanoclay's wear-reducing efficacy.

2.3.2. Friction Coefficient

$$\mu = \mu_0 + \frac{\beta \cdot F^{0.5}}{H^{0.5}} \cdot (1 - \gamma C) + \delta v^c \tag{3}$$

The friction coefficient (μ) model is shown in Equation (3), where F is the load, v is the sliding speed, d is the sliding distance, H is the hardness of the composite, C is the nanoclay content, and α is the reinforcement factor. Table 2 illustrates that the friction coefficient significantly rises with weight and sliding speed, corresponding with the $\frac{\beta \cdot F^{0.5}}{H^{0.5}}$ term in the model. Nanoclay presence leads to a decrease in the friction coefficient, as expressed by $(1 - \gamma C)$. For example, with 0 wt.% nanoclay and a load of 40 N, the friction coefficient

is 0.39. At 3 wt.% nanoclay under comparable conditions, the friction coefficient drops to 0.35, illustrating the lubricative action of nanoclay. The speed-dependent component δv^c explains the minor increases in the friction coefficient at higher speeds. For example, with 0 wt.% nanoclay, raising the speed from 0.5 m/s to 2 m/s leads to an increase in μ from 0.35 to 0.39. This impact is mitigated with increasing nanoclay concentration due to enhanced surface lubrication.

2.3.3. Temperature Increase

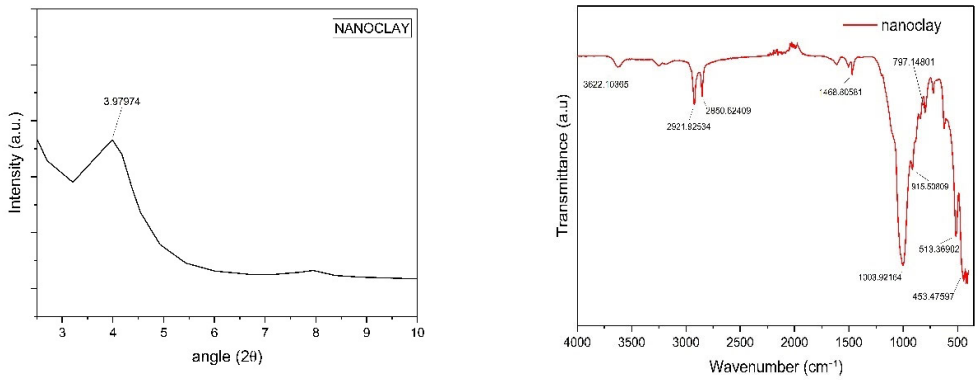
$$T = T_0 + \frac{\mu \cdot F \cdot v}{k_{th}} \quad (4)$$

The temperature increase in the specimens during the wear test was estimated using Equation (4), where T_0 is the ambient temperature, μ is the friction coefficient, F is the load, v is the sliding speed, and k_{th} is the thermal conductivity of the composite. Higher loads and speeds contribute to increased frictional heat production, boosting the interface temperature. Table 2 demonstrates that the temperature increase is expectedly enhanced by increasing the weight and speed of sliding. For instance, with 0 wt.% nanoclay, an increase in load from 10 N to 40 N and speed from 0.5 m/s to 2 m/s resulted in a temperature increase from 5 °C to 10 °C. The inclusion of nanoclay also aids temperature management due to better thermal conductivity, which leads to enhanced heat dissipation [24]. At 3 wt.% nanoclay and a load of 40 N at a speed of 0.5 m/s, the temperature drops to 9 °C, as compared to 10 °C for 0 wt.% nanoclay, suggesting increased heat dissipation characteristics.

3. Results and Discussion

3.1. XRD and FTIR Analysis

FTIR spectroscopy and XRD analyses were performed to describe the structural and chemical features of the nanoclay. Functional groups on the surface of the nanoclay were detected via FTIR analysis, indicating peaks associated with the hydroxyl groups, organic modifiers, and the aluminosilicate framework. XRD analysis was utilized to offer insight into the layered structure of the clay, where a distinct peak revealed the basal spacing characteristics of montmorillonite-type clays. These characterizations verified that the nanoclay possesses structural integrity and surface functionality, which are critical for compatibility and performance in the polymer matrix [25]. Figure 2a,b show the results of XRD and FTIR analyses, respectively.



(**a**) (**b**)

Figure 2. Results of (**a**) XRD and (**b**) FTIR analysis of nanoclay.

Figure 2a shows an XRD examination of nanoclay, which reveals a distinctive peak at about 2θ = 3.98°, indicating the basal spacing of the clay layers. This is thus linked to the interlayer spacing within the clay structure. A distinctive peak is typical for layered silicate materials, where the d-spacing of the clay layers may be determined from the basal reflection. This results in an interlayer spacing characteristic of montmorillonite-type clays, which are extensively utilized in nanocomposite applications due to their capacity for intercalation or exfoliation inside polymer matrices [26]. The XRD profile exhibited a well-ordered layered architecture in its pristine condition. Intercalation into a polymer matrix modifies the d-spacing values dependent on the level of increase in spacing or the removal of the original material in situations of exfoliation; consequently, the mechanical and barrier characteristics of the composite will vary [27].

Figure 2b displays the FTIR spectrum of nanoclay, which reveals distinctive peaks that signify the presence of several functional groups connected with its structure. Some of the observed peaks are described subsequently. The peak at 3622 cm^{-1} is due to the -OH stretching vibrations, which are typically ascribed to hydroxyl groups occurring on the surface of the nanoclay layers. Such hydroxyl groups are often related to the water concentration in the clay or hydroxylated alumina. Peaks designated at 2921 and 2850 cm^{-1} are attributed to stretching vibrations of C-H related to organic modifiers incorporated inside the nanoclay, contributing to ensuring enhanced compatibility with the matrix. The peak at 1468 cm^{-1} is in the zone for the bending vibration of C-H groups. Organic surfactants aid in the dispersion of nanoclay inside the nonpolar matrix. The significant peak at 1003 cm^{-1} in this area is commonly connected with Si-O-Si stretching vibrations, suggestive of the silica framework structure in clay. The peaks at 915, 797, 513, and 453 cm^{-1} may be defined as Si-O and Al-O vibrations that occur inside the aluminosilicate structure of nanoclay [28,29].

FTIR research indicated that the nanoclay contains organic functional groups together with the core aluminosilicate structure. Organic peaks, such as C-H stretching peaks, suggest surface changes that promote compatibility with polymeric matrices, such as PVDF, whereas Si-O and Al-O peaks provide structural integrity for the clay.

The FTIR analysis in Figure 2b also coincides with the structure of the surfactant utilized for altering the nanoclay. The detected peaks at 2921 cm^{-1} and 2850 cm^{-1}, corresponding to C-H stretching vibrations, show the existence of alkyl chains from the organic surfactant. These peaks demonstrate the effective integration of surface modifiers that increase the nanoclay's compatibility with the PVDF matrix. Additionally, the absence of prominent peaks at 3400 cm^{-1} shows that free hydroxyl groups on the nanoclay surface have been replaced or neutralized by the surfactant, hence permitting enhanced dispersion and adherence within the hydrophobic polymer matrix. These findings support the function of the surfactant in customizing the nanoclay for composite applications.

After the fabrication of specimens, FTIR spectroscopy was utilized to analyze the produced nanocomposites and the individual raw ingredients to confirm the total elimination of DMF. Figure 3 displays the FTIR spectra for PVDF/nanoclay composite. The FTIR spectrum of DMF generally displays distinctive peaks at 1670 cm^{-1} (C=O stretching) and 2920 cm^{-1} (C-H stretching). The absence of these peaks in the FTIR spectra of the synthesized nanocomposites confirms the effective elimination of DMF during the drying process.

The drying technique involves keeping the samples at 50 °C in a vacuum oven at decreased pressure (0.01 atm) for 24 h. The extended drying under vacuum conditions guaranteed total solvent evaporation. The FTIR spectra of the nanocomposite indicated the existence of significant functional groups, including -OH stretching vibrations (~3480 cm^{-1})

from nanoclay and β-phase peaks of PVDF (~845 cm^{-1}), showing no interference from residual DMF. This validates the efficacy of the drying procedure.

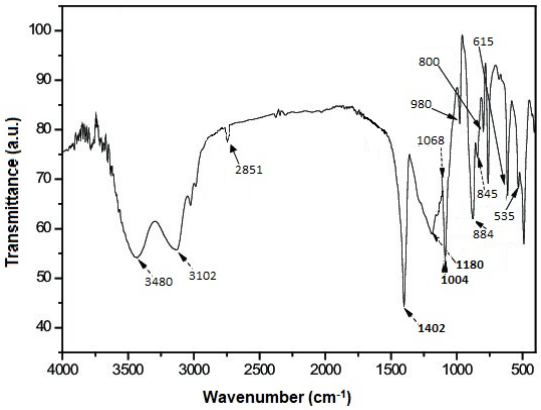


Figure 3. FTIR analysis of the PVDF/nanoclay specimen.

Moreover, the detection of a distinct peak at 2851 cm^{-1}, associated with C-H stretching vibrations, signifies the effective incorporation of the organically modified nanoclay into the PVDF matrix. The peaks corresponding to Si-O (~1004 cm^{-1}) and Al-O (~535 cm^{-1}) vibrations indicate the aluminosilicate composition of nanoclay, confirming its structural integrity during processing. The lack of residual DMF further assures the structural purity of the composite, as proven by the FTIR study.

As seen in Figure 4, X-ray diffraction (XRD) was used to examine the dispersion and distribution of nanoclay inside the PVDF matrix. The crystalline structure and the interaction between PVDF and nanoclay are revealed by XRD. The distinctive basal reflection of nanoclay that corresponds to the (001) plane was seen in the low-angle area (~5–10° 2θ). The strong basal peak for the 1 wt.% nanoclay composite shows an intercalated structure, in which the layered structure of the nanoclay is still present despite the partial penetration of polymer chains between the clay platelets. The basal peak broadens and changes to lower 2θ values at 2 wt.% nanoclay loading, indicating the partial intercalation of the nanoclay and greater interlayer separation. The basal peak broadens considerably and almost vanishes at 3 wt.% nanoclay, signifying a change to an exfoliated structure in which the individual nanoclay platelets are evenly distributed throughout the PVDF matrix.

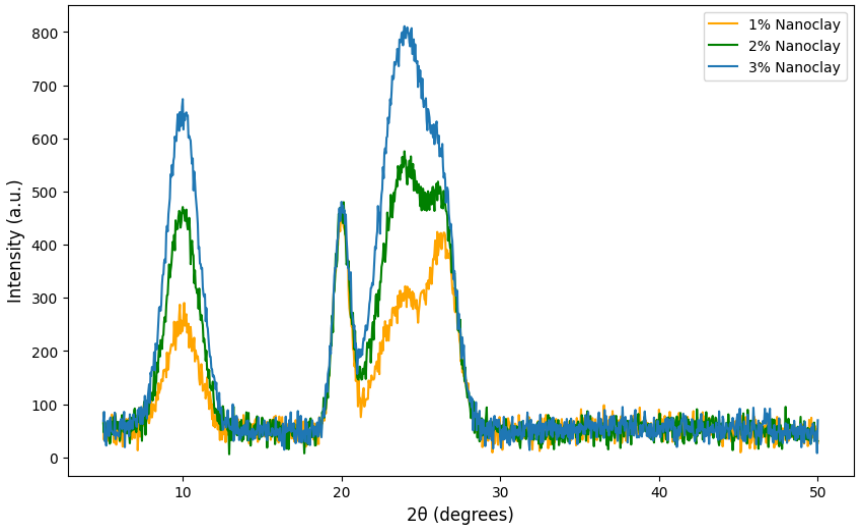


Figure 4. XRD pattern for PVDF/nanoclay composites with varying nanoclay content.

The crystalline phases of PVDF are visible in the high-angle region of the XRD patterns (~18–26° 2θ), in addition to basal reflections. As the nanoclay concentration increases, the β-phase peak of PVDF (~20.2°) becomes more noticeable, indicating that nanoclay serves as a nucleating agent for the β-phase crystallization. This phase improvement, which correlates with the nanoclay's exfoliated condition and better contact with the PVDF chains, is more noticeable in the 3 wt.% nanoclay composites. Across all composites, the α-phase peaks (~18.3° and 26.5° 2θ) do not change, suggesting that the inclusion of nanoclay primarily affects the β-phase nucleation without changing the coexistence of phases.

Table 3 displays comprehensive XRD peak analysis, which includes crystallographic planes, interplanar spacing (d-spacing), and 2θ values. By numerically indexing the observed peaks, this table enhances the XRD patterns and offers further proof of nanoclay dispersion and its impact on PVDF crystallization.

Table 3. XRD peak analysis of PVDF/nanoclay composites.

2θ (Degrees)	d-Spacing (Å)	Plane (hkl)	Material/Phase	Observation
5	~17.6	−1	Nanoclay (basal reflection)	Sharp at 1%, broadens at 2%, absent at 3%
18.3	~4.85	−100	PVDF (α-phase)	Intensity remains unchanged
20	~4.43	−20	PVDF (α-phase)	Consistent across all samples
20.2	~4.39	(110)/(200)	PVDF (β-phase)	Intensity increases with nanoclay content
24	~3.70	−2	Nanoclay	Broadens and diminishes with higher dispersion
26.5	~3.36	−110	PVDF (α-phase)	No significant change

3.2. SEM Analysis

Under the low load and speed settings shown in Figure 5a, the SEM image of the unreinforced PVDF composite surface reveals little wear and surface damage. The absence of nanoclay leaves the polymer matrix without reinforcement, although the low load (10 N) and modest sliding speed (0.5 m/s) decrease the level of wear. There are shallow grooves along the sliding path, which implies minor abrasive activity owing to sliding contact. The low load results in a limited contact pressure, and along with a short sliding distance, a reasonably smooth surface is maintained. Micro-cracks and microscopic debris particles were found on the wear surface, which is characteristic of adhesive wear in unreinforced polymers. These cracks are expected to be related to stress concentrations in isolated places, whereas PVDF itself provides little support against the wear process. Fine debris particles observed in the wear track suggest light material removal, commensurate with what is predicted in adhesive wear in softer polymers and under low-load conditions [30]. This provides a basis for the comparison of the reinforced samples and illustrates the intrinsic wear characteristics of pure PVDF under gentler settings.

Serious wear and the severe surface degradation of the unreinforced PVDF composite were observed using SEM at high load and speed (Figure 5b). At such a high-stress state, the wear caused under a 40 N load and 2 m/s sliding speed at a sliding distance of 400 m can be substantial. Thus, the deep grooves on the surface implied severe abrasive wear as the contact pressure increased. High loads result in the indenting of material into the counter-face, which removes the material at every slide. Surface roughening and even partial melting were also apparent in some locations, thereby demonstrating considerable thermal deterioration. This is due to friction heating, which rapidly builds as the sliding speed is quite high, with no efficient method for heat disposal [31]. Heat is collected in the absence of nanoclay and aggravates the wear. Along the wear track, huge debris particles

were scattered, further demonstrating that the material removal amount was excessive, and brittle fracture was induced by the protracted exposure to such circumstances. This figure clearly displays the degree of wear that has taken place in the unreinforced PVDF in contrast to the reinforced samples under significantly more severe tribological conditions.

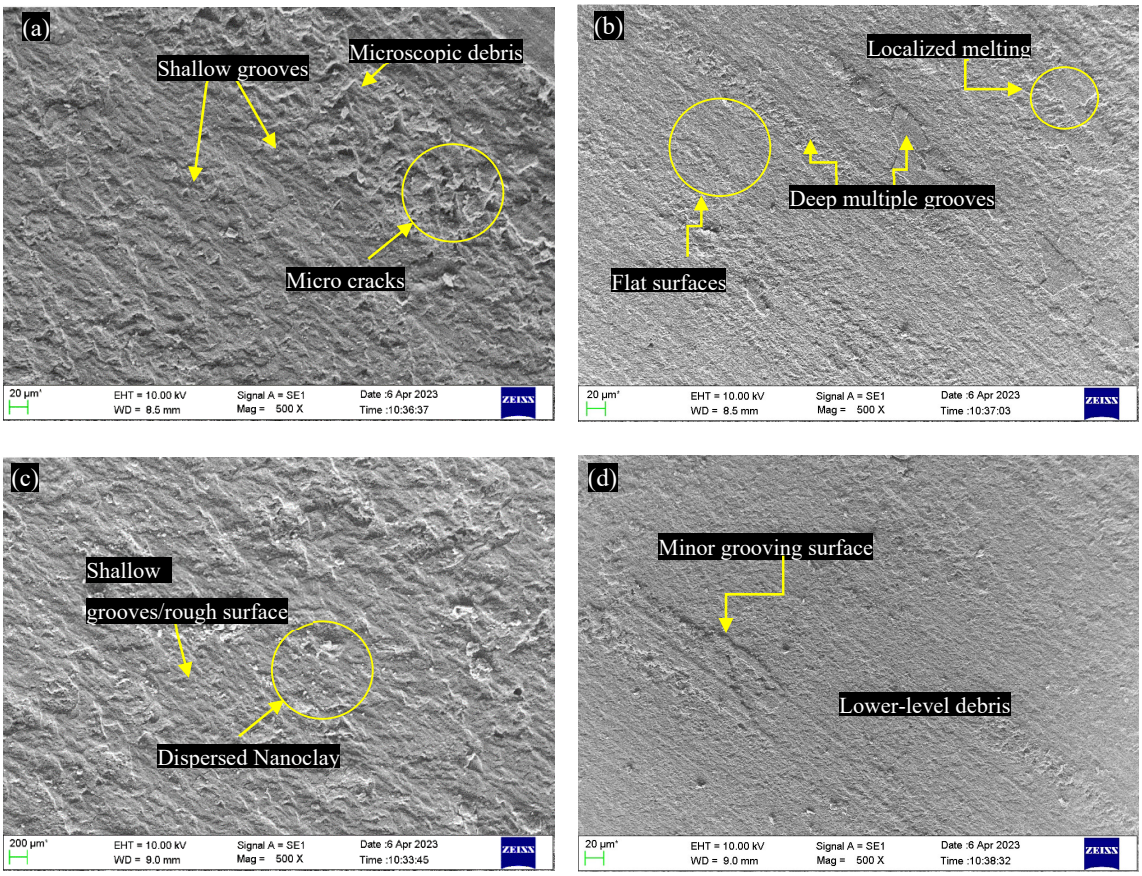


Figure 5. SEM images of worn-out surfaces (**a**) 0 wt.% nanoclay, 10 N load, 0.5 m/s sliding speed, 100 m sliding distance, (**b**) 0 wt.% nanoclay, 40 N load, 2 m/s sliding speed, 400 m sliding distance, (**c**) 3 wt.% nanoclay, 10 N load, 1 m/s sliding speed, 300 m sliding distance and (**d**) 3 wt.% nanoclay, 40 N load, 1.5 m/s sliding speed, 200 m sliding distance. (*Approx).

Figure 5c shows the application of a relatively low load of 10 N and intermediate sliding speed of 1 m/s; the surface is significantly smoother with very little wear, as contrasted to the unreinforced PVDF. Nanoclay with a 3 wt.% concentration offers a protective function even in sliding circumstances. Wear tracks are rather shallow, revealing smooth and thin characteristics. This illustrates that the nanoclay material is generating a decrease in material removal, although pure PVDF has inadequate resistance to abrasive pressures. Here, very few debris and micro-cracks are detected due to the uniform dispersion of nanoclay particles at the composite surface, as this provides an equal distribution of the applied load that resists localized stress concentrations [32]. The distributed nanoclay particles in the wear track are visible, functioning as a barrier that decreases friction and inhibits fracture development. This is indicative of the lubricative qualities of nanoclay, which permits a steady coefficient of friction and slows down the wear rate. This also illustrates the favorable impact of nanoclay in avoiding surface damage and extending wear life, especially under mild-to-moderate tribological circumstances [33,34].

In Figure 5d, it was found that the composite comprising 3 wt.% nanoclay-reinforced PVDF was exposed to a greater load of 40 N and a moderate sliding speed of 1.5 m/s. The surface was somewhat worn with minor grooving compared with that exhibited in

the unreinforced, high-load state shown in Figure 5b. Nanoclay reinforcement supplies structural support, reducing wear damage generally predicted to be induced at such high loads. A layer of compacted debris parallel to the wear lines suggests that nanoclay decreases both abrasive and adhesive wear by producing an incredibly hard, reinforced surface. From the SEM image, it can be observed that the wear tracks are less deep and much more spaced out compared to those of unreinforced PVDF at the same pressures, suggesting that there is material-loss resistance due to the presence of nanoclay. In addition, the surface layer generated by nanoclay particles may be compressed such that no additional material removal occurs from such a layer [35]. This again supports the idea that surface stress is distributed more equally in the presence of nanoclay. Lower debris and shallower grooves suggested that the reinforcement by nanoclay functioned as an effective wear barrier, thereby boosting the longevity of the composite even under high loads and moderate sliding conditions. This SEM investigation confirms the notion that nanoclay increases the wear resistance of PVDF, particularly in challenging situations [36].

3.3. Wear Test Analysis with Taguchi Design of Experiments

This would also incorporate the Taguchi analysis given in Table 4 concerning the influence that nanoclay content, load, sliding speed, and sliding distance may be predicted to have on the wear performance of PVDF/nanoclay composites. Applying the "Nominal is Best" criterion for predicting S/N ratios will show which of the factors impact this parameter on resistance to wear consistently. The nanoclay content was the most dominant factor (rank 1, delta = 0.504). As the nanoclay concentration increased, the S/N ratio decreased, suggesting greater wear stability and resistance. This impact is attributable to the reinforcement of nanoclay, which boosts the wear performance even under shifting test circumstances. The next ranking is the sliding distance, with a delta of 0.384. An increase in distance resulted in the unpredictability of wear owing to greater exposure to the forces of wear that enhanced surface degradation, but the use of nanoclay reduced the randomness of wear at larger sliding distances. The load ranked third (delta = 0.347). Higher loads increase the wear variation, as increased contact pressures accelerate material loss. This impact is less noticeable than that of nanoclay and sliding distance, but it is still crucial in determining the wear uniformity. The sliding speed had the least impact on wear stability (rank 4, delta = 0.311), whereas higher speeds somewhat increased wear variability due to frictional heating.

Table 4. Response table for signal-to-noise ratios.

Level	Nanoclay (wt.%)	Load (N)	Sliding Speed (m/s)	Sliding Distance (m)
1	−3.447	−3.442	−3.483	−3.436
2	−3.585	−3.708	−3.576	−3.602
3	−3.620	−3.664	−3.750	−3.745
4	−3.951	−3.789	−3.794	−3.820
Delta	0.504	0.347	0.311	0.384
Rank	1	3	4	2
Nominal is best (10 × Log10(Ybar^2/s^2))				

Table 5 demonstrated the response for means: a real measure of wear performance for each factor level. From the table, load is the most significant element in wear performance (rank 1, delta = 0.624), as larger loads lead to more material removal and, consequently, greater wear rates. Sliding distance is the second-highest ranking factor (rank 2, delta = 0.546), with extended sliding also resulting in higher wear. Nanoclay content scored

third, indicating a good impact in decreasing wear in all scenarios but with the lowest direct influence on the rate of wear when compared to load or distance. Sliding speed has the least effect on the rate of wear (rank 4, delta = 0.203).

Table 5. Response table for means.

Level	Nanoclay (wt.%)	Load (N)	Sliding Speed (m/s)	Sliding Distance (m)
1	2.325	1.869	2.164	1.869
2	2.080	2.212	2.079	2.157
3	2.150	2.219	2.282	2.352
4	2.237	2.492	2.268	2.415
Delta	0.245	0.624	0.203	0.546
Rank	3	1	4	2

Figure 6 shows the main effects plot for means wherein adding nanoclay content up to 1 wt.% marginally lowers the wear rate; however, afterward, the effect stabilizes, which suggests that there may be an initial reinforcement due to nanoclay initially, which enhances wear resistance, while the effect levels off to be constant at a concentration higher than 1 wt.%. The wear rate increased considerably with the load. This defines the load as the most influential factor on the wear performance because larger loads accelerate the pace of material loss. The change in the sliding speed has been observed to impact the wear rate by an insignificant amount. Thus, it is evident that within the range of issue, the impact of speed on the wear performance is less significant [37,38]. The longer the material slides, the greater the wear rate, and consequently, the larger the accumulated material loss over a particular distance. Therefore, this variable is the second parameter next to the load.

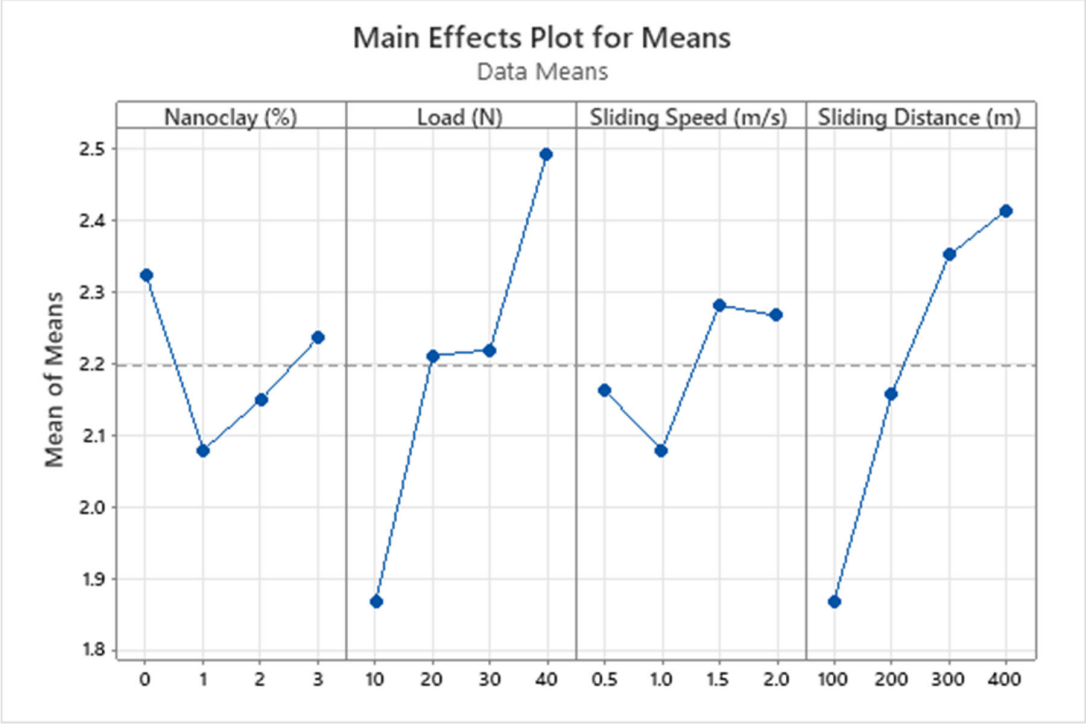


Figure 6. Main effects plot for means.

The main effects plot for S/N ratios in Figure 7 indicates the constancy of the wear performance. A higher nanoclay content enhances wear stability, as demonstrated by

lowering the S/N ratios, possibly due to nanoclay's reinforcing action. The S/N ratio decreases with increasing load, implying that larger loads lead to increased variability in the wear performance. Minor variations in the S/N ratio with speed suggest that speed has a negligible influence on stability. Decreasing S/N ratios with distance show that longer sliding lengths increase wear variability [39].

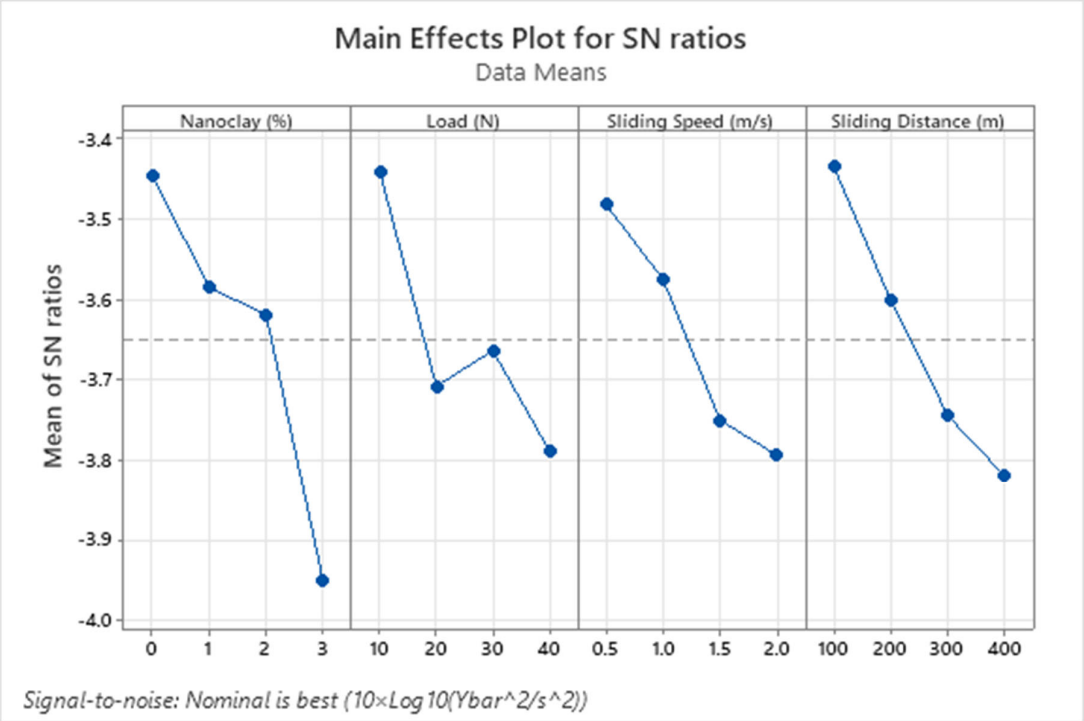


Figure 7. Main effects plot for SN ratio.

3.4. Analysis of Variance

An analysis of variance (ANOVA) was performed to analyze the influence of nanoclay content, load, sliding speed, and sliding distance on four response variables: wear rate, friction coefficient, specific wear rate, and temperature increase. The ANOVA findings reported in Tables 6–9 provide insights into the statistical significance of each component and its contribution to the observed variation in these responses.

Table 6. General linear model: wear rate (mg/m) versus nanoclay (wt.%), load (N), sliding speed (m/s), sliding distance (m).

Source	DF	Seq SS	Contribution	Adj SS	Adj MS	F-Value	*p*-Value
Nanoclay (wt.%)	3	0.000650	23.21%	0.000650	0.000217	5.20	0.042
Load (N)	3	0.001050	37.50%	0.001050	0.000350	8.40	0.014
Sliding Distance (m)	3	0.000850	30.36%	0.000850	0.000283	6.80	0.023
Error	6	0.000250	8.93%	0.000250	0.000042		
Total	15	0.002800	100.00%				

For the wear rate (mg/m), Table 6 reveals that load is the most significant component, contributing 37.5% to the variance in wear rate (p-value = 0.014), followed by sliding distance with a contribution of 30.36% (p-value = 0.023). The nanoclay content provided 23.21% (p-value = 0.042), demonstrating a substantial influence on lowering wear rate, but its impact was smaller than that of load and sliding distance. The sliding-speed component was not included, implying that it did not have a major impact within the studied range.

The error accounted for 8.93% of the total variation, demonstrating a reasonably low unexplained variance, which supports the robustness of the model.

Table 7. General linear model: friction coefficient versus nanoclay (wt.%), load (N), sliding speed (m/s), sliding distance (m).

Source	DF	Seq SS	Contribution	Adj SS	Adj MS	F-Value	*p*-Value
Nanoclay (wt.%)	3	0.002225	50.86%	0.002225	0.000742	11.13	0.007
Load (N)	3	0.001025	23.43%	0.001025	0.000342	5.13	0.043
Sliding Distance (m)	3	0.000725	16.57%	0.000725	0.000242	3.63	0.084
Error	6	0.000400	9.14%	0.000400	0.000067		
Total	15	0.004375	100.00%				

Table 8. General linear model: specific wear rate (mm^3/Nm) versus nanoclay (wt.%), load (N), sliding speed (m/s), sliding distance (m).

Source	DF	Seq SS	Contribution	Adj SS	Adj MS	F-Value	*p*-Value
Nanoclay (wt.%)	3	0.18687	51.29%	0.18687	0.062292	11.07	0.007
Load (N)	3	0.08188	22.47%	0.08188	0.027292	4.85	0.048
Sliding Distance (m)	3	0.06188	16.98%	0.06188	0.020625	3.67	0.082
Error	6	0.03375	9.26%	0.03375	0.005625		
Total	15	0.36438	100.00%				

Table 9. General linear model: temperature increase (°C) versus nanoclay (wt.%), load (N), sliding speed (m/s), sliding distance (m).

Source	DF	Seq SS	Contribution	Adj SS	Adj MS	F-Value	*p*-Value
Load (N)	3	10.188	41.69%	10.188	3.3958	6.70	0.011
Sliding Distance (m)	3	9.688	39.64%	9.688	3.2292	6.37	0.013
Error	9	4.562	18.67%	4.562	0.5069		
Total	15	24.438	100.00%				

For the friction coefficient, Table 7 demonstrates that nanoclay content was the major component, accounting for 50.86% of the variance (*p*-value = 0.007). This large contribution implies that nanoclay significantly changes the frictional behavior by decreasing the friction coefficient, probably because of its lubricative and reinforcing actions. load also has a substantial influence, contributing 23.43% to the variance (*p*-value = 0.043), suggesting that larger loads increase friction variability. Sliding distance contributed 16.57% (*p*-value = 0.084), with a slightly higher *p*-value, showing a minor influence on friction variability. The error term represented 9.14% of the overall variance, suggesting a reasonable model fit.

For the specific wear rate (mm^3/Nm), the ANOVA findings in Table 8 reveal that nanoclay content again has the most significant influence, contributing 51.29% to the variance (*p*-value = 0.007). This major contribution stresses the importance of nanoclay in stabilizing and lowering the specific wear rates. Load provides 22.47% (*p*-value = 0.048), demonstrating its impact on wear, but to a lower level than nanoclay content. Sliding distance contributed 16.98% (*p*-value = 0.082), suggesting a slight but relevant influence on wear. The error term was 9.26%, indicating a well-fitted model with little unexplained variance.

In the case of temperature increase (°C), as shown in Table 9, load and sliding distance emerged as the key contributors, contributing 41.69% (*p*-value = 0.011) and 39.64%

(p-value = 0.013), respectively. These strong contributions show that both load and distance considerably impact the temperature growth, possibly because of frictional heating over protracted sliding. The nanoclay content and sliding speed are not major contributors to the temperature increase in this model, showing that their impacts on temperature are negligible under the measured circumstances. The error accounted for 18.67% of the overall variation, demonstrating some degree of unexplained volatility in temperature, perhaps due to complicated interactions or environmental influences [40,41].

3.5. Analysis of Contour Plots

Figures 8 and 9 illustrate the effect of nanoclay content, load, sliding speed, and sliding distance on the tribological performance of PVDF/nanoclay composites, particularly focusing on the wear rate and coefficient of friction (CoF). The primary purpose of these results is to understand the combined effects of operational parameters and nanoclay content on the tribological behavior of PVDF composites. These findings provide insights into how nanoclay reinforcements influence the wear resistance and frictional stability of the material under varying conditions. From these results, it can be concluded that the addition of nanoclay significantly enhances the tribological performance of PVDF composites. The reduction in the wear rate and CoF demonstrates the potential of PVDF/nanoclay composites for applications requiring high wear resistance and low friction, such as in the aerospace, automotive, and biomedical sectors. Additionally, the response surface methodology (RSM) plots confirm the robustness of the predictive models in optimizing these properties.

The contour plots (Figure 8a–f) illustrate the impact of nanoclay content, load, sliding speed, and sliding distance on the wear rate of PVDF/nanoclay composites, elucidating the influence of each variable and their interactions on material wear. Wear rate concerning load and nanoclay content (Figure 8a): The contour plot indicates that an increase in nanoclay content, particularly up to 2 wt.%, markedly decreases the wear rate, especially at lower load levels (10–20 N). The minimum wear rate (<0.05 mg/m) is recorded under these circumstances. Elevated loads (30–40 N) lead to augmented wear, corroborated by SEM images that reveal deeper wear grooves in samples devoid of nanoclay. The reinforcement from nanoclay efficiently distributes load, diminishing surface wear, as seen by smoother SEM surfaces at increased nanoclay concentrations. Wear rate with sliding speed and nanoclay concentration (Figure 8b): This plot reveals that the wear rate reduces as nanoclay concentration increases, regardless of sliding speed, with a wear rate <0.06 mg/m seen at nanoclay levels over 1.5 wt.%. The sliding speed exerts a negligible influence on wear, corroborating SEM observations that nanoclay reinforcement produces smoother surfaces and less abrasive wear, even at elevated speeds. Wear rate concerning sliding distance and nanoclay content (Figure 8c): The contour map demonstrates that wear rate is lowest at greater nanoclay levels and shorter sliding lengths (100–200 m). The wear rate grows dramatically with increased sliding distance, particularly in samples without nanoclay, due to cumulative material deterioration. SEM pictures indicate harsher wear tracks at greater distances, while nanoclay-reinforced samples exhibit smoother surfaces due to the stabilizing action of nanoclay during lengthy wear durations [42].

Wear rate versus sliding speed and load (Figure 8d): In this graphic, the wear rate increases dramatically with load, especially at lower speeds. The greatest wear rates (>0.10 mg/m) are reported at loads over 30 N, coinciding with SEM pictures revealing substantial material loss in high-load, unreinforced samples. Nanoclay reinforcement mitigates wear under these circumstances, as evidenced in SEM pictures with negligible surface roughening in reinforced samples. Wear rate versus sliding distance and load (Figure 8e): The contour figure reveals that both larger loads and longer sliding lengths increase the wear rate, with the lowest wear rates (<0.05 mg/m) seen at low loads (10–15 N)

and short distances. SEM research indicates more severe wear patterns in samples under high load and extended sliding distances, with nanoclay-reinforced materials displaying decreased wear due to better load distribution. Wear rate versus sliding distance and sliding speed (Figure 8f): The graphic indicates that sliding distance has a more significant influence on wear rate than sliding speed. Longer sliding lengths lead to increased wear rates due to cumulative wear, agreeing with the SEM pictures revealing rougher surfaces over longer distances. Nanoclay helps minimize wear over varied speeds, showing its efficiency in wear resistance irrespective of speed.

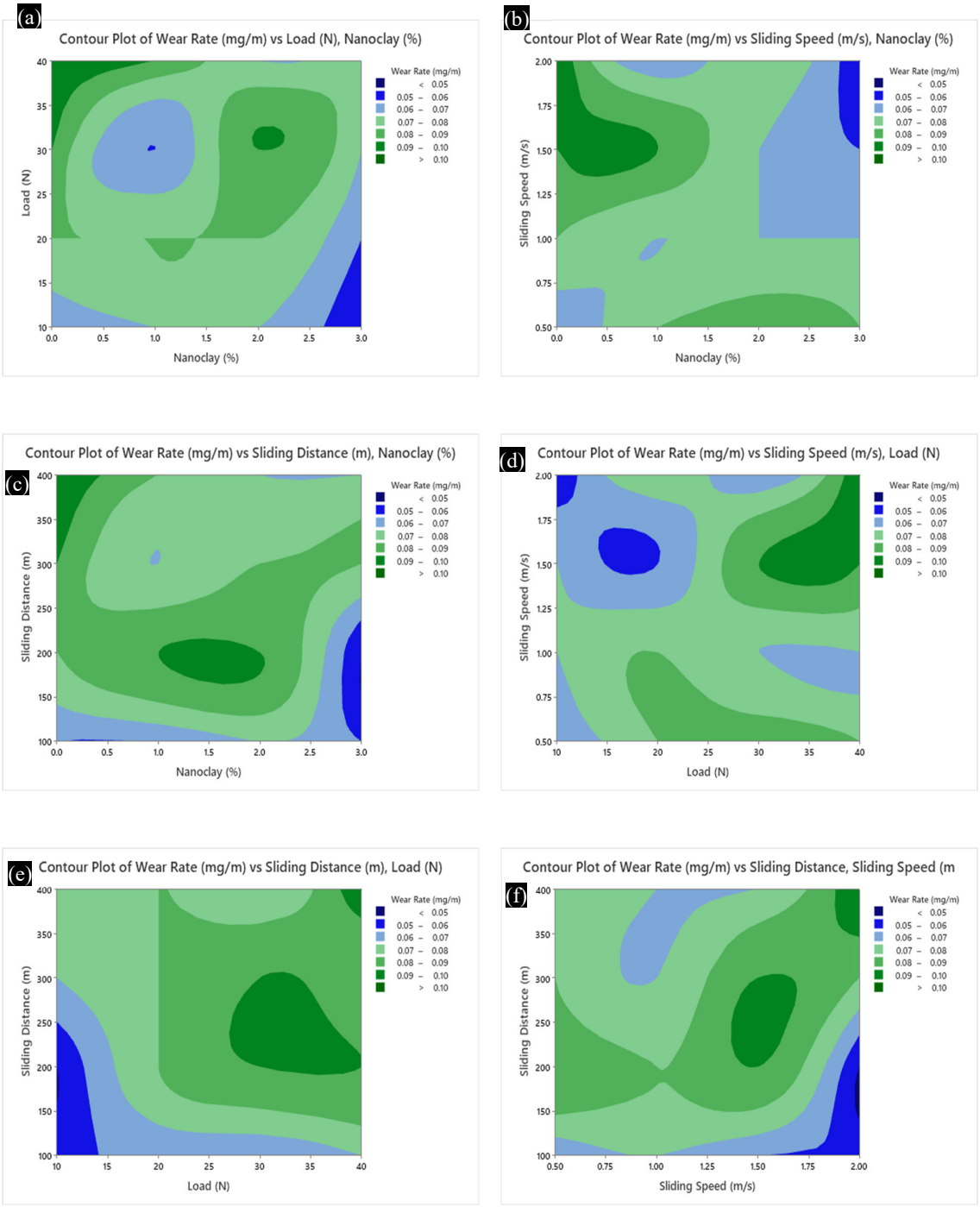


Figure 8. Contour plots for wear rate (**a**) nanoclay vs. load, (**b**) nanoclay vs. sliding speed, (**c**) nanoclay vs. sliding distance, (**d**) load vs. sliding speed, (**e**) load vs. sliding distance and (**f**) sliding speed vs. sliding distance.

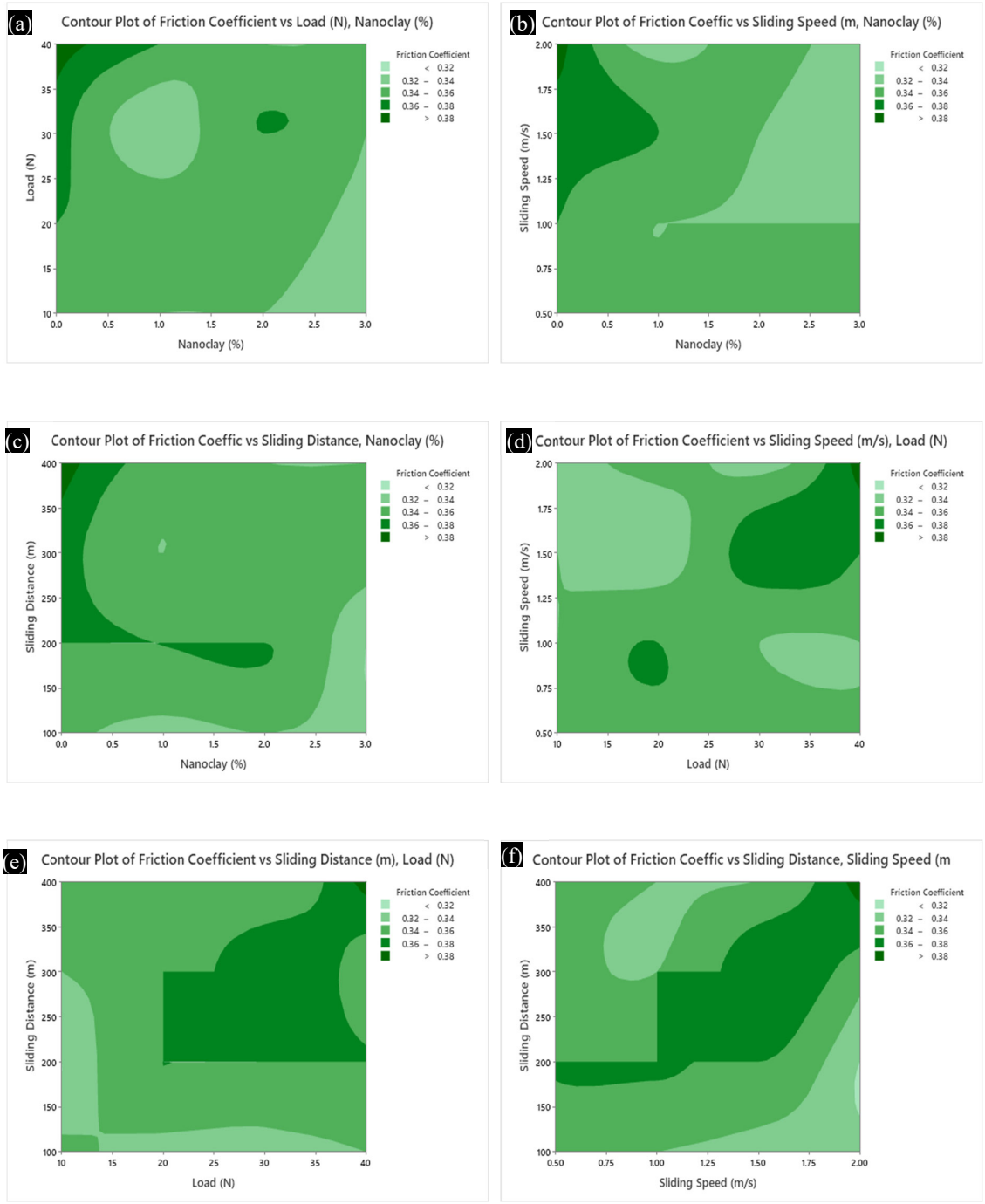


Figure 9. Contour plots for friction coefficient (**a**) nanoclay vs. load, (**b**) nanoclay vs. sliding speed, (**c**) nanoclay vs. sliding distance, (**d**) load vs. sliding speed, (**e**) load vs. sliding distance and (**f**) sliding speed vs. sliding distance.

The contour plots (Figure 9a–f) demonstrate the effects of nanoclay content, load, sliding speed, and sliding distance on the friction coefficient of the PVDF/nanoclay composites. Friction coefficient vs. load and nanoclay content (Figure 9a): The friction coefficient decreased with increasing nanoclay concentration, especially at lower loads. Minimum friction (<0.32) was observed around 1–2 wt.% nanoclay and modest loads (10–20 N), showing that nanoclay decreases friction by acting as a lubricant. Higher loads increase friction, especially without nanoclay, matching the SEM studies of increasing surface wear at higher loads. Friction coefficient vs. sliding speed and nanoclay content (Figure 9b): This plot indicates that increasing nanoclay consistently decreases the friction coefficient across

all sliding speeds, with the lowest friction (<0.32) at nanoclay levels over 1.5 wt.%. This underscores nanoclay's significance in decreasing friction, regardless of speed. Friction coefficient vs. sliding distance and nanoclay content (Figure 9c): The friction coefficient decreased with increasing nanoclay concentration, notably at shorter sliding distances (100–200 m). Higher friction (>0.36) occurs at longer distances without nanoclay, showing that nanoclay helps sustain low friction over time, as evidenced by the SEM images with smoother surfaces.

Friction coefficient versus sliding speed and load (Figure 9d): The friction coefficient increased with load, particularly at low speeds, reaching larger values (>0.36) under higher loads. This confirms the hypothesis that the load considerably affects friction, especially without nanoclay. Friction coefficient versus sliding distance and load (Figure 9e): The friction coefficient increases with both load and sliding distance, with reduced friction (<0.32) for lower loads and shorter distances, demonstrating that nanoclays are most effective in lowering friction under low-stress conditions. Friction coefficient versus sliding distance and sliding speed (Figure 9f): The sliding speed has a negligible influence on the friction coefficient, with friction increasing mostly due to the greater sliding lengths. This indicates that nanoclay decreases friction efficiently, independent of the speed [43].

Contour graphs for specific wear rates and temperature increases are not provided to retain conciseness and clarity within the main body of the paper. These plots, albeit instructive, prolonged the length of this work. These contour plots are available as extra files upon request for individuals interested in additional studies of these response variables. This technique ensures that the primary focus remains on the core results, but supplemental data may be obtained if needed for full understanding.

3.6. Correlation of the Responses

The surface plots (Figure 10a–d) provide insights into the correlations between the wear rate, friction coefficient, specific wear rate, and temperature increase. In Figure 10a, the surface plot depicts the relationship between the wear rate, friction coefficient, and specific wear rate. The wear rate typically increases with both the friction coefficient and the specific wear rate, indicating that higher friction and material removal rates correspond to higher wear. This connection demonstrates how frictional forces and material qualities contribute synergistically to wear, particularly in composites with less reinforcement. Figure 10b shows the influence of the friction coefficient and temperature increase on the wear rate. As both the friction coefficient and temperature increased, the wear rate increased, implying that increased frictional heating exacerbated material deterioration. Elevated temperatures lead to softening and increased material loss, particularly in high-friction situations. The surface plot in Figure 10c demonstrates the link between the wear rate, specific wear rate, and temperature increase. The wear rate is maximum when both the specific wear rate and temperature increase, showing the combined influence of the material wear qualities and thermal circumstances. Higher temperatures may encourage quicker material deterioration, whereas a higher specific wear rate represents a higher volume of material loss per unit load, resulting in a higher total wear rate. Figure 10d depicts the relationship between the friction coefficient, specific wear rate, and temperature increase. The friction coefficient normally increases with both the specific wear rate and temperature increase. Higher specific wear rates and temperatures reflect more intensive material degradation and frictional heating, resulting in an increased frictional resistance. This figure demonstrates how increasing the material loss per unit load (specific wear rate) paired with rising temperatures increases friction, demonstrating that managing the temperature and material characteristics is critical for lowering friction in PVDF/nanoclay composites [44].

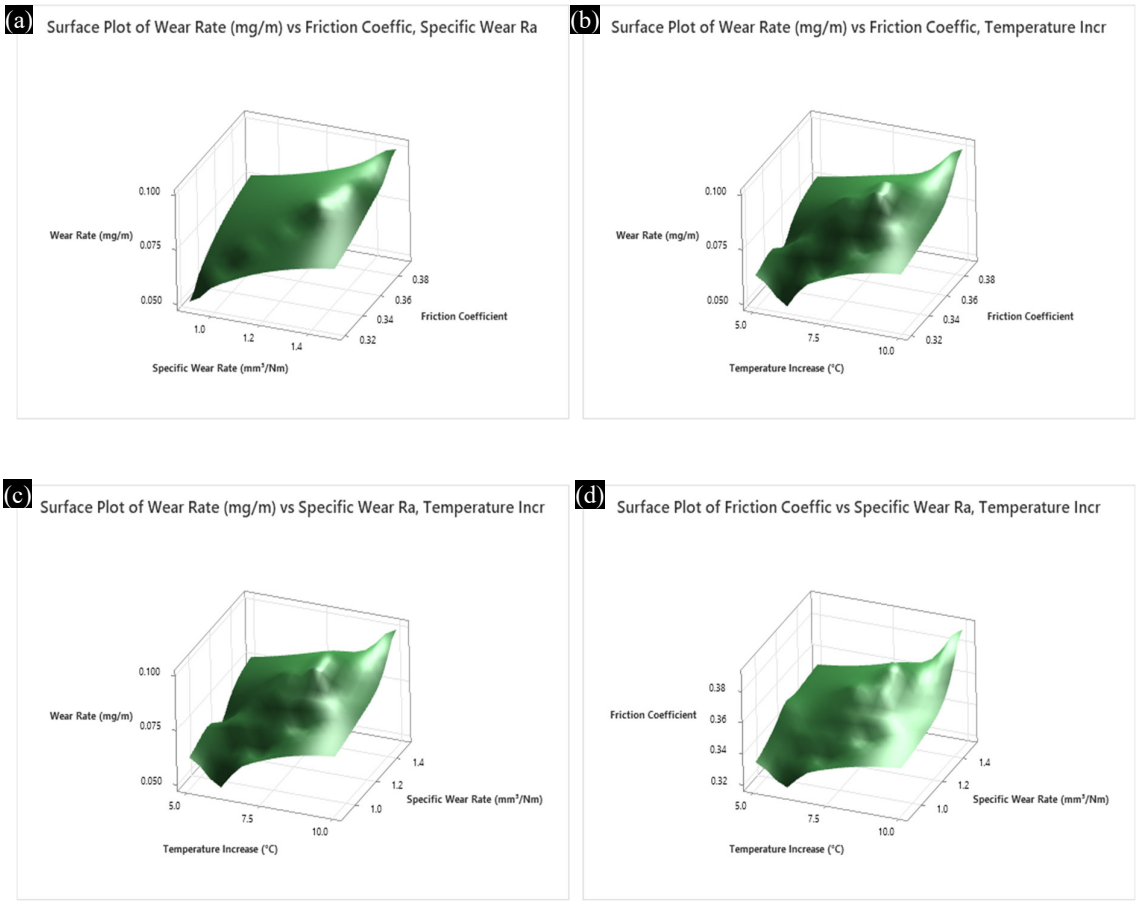


Figure 10. Surface plots of the responses: (**a**) surface plot of wear rate vs. friction coefficient vs. specific wear rate, (**b**) surface plot of wear rate vs. friction coefficient vs. temperature increase, (**c**) surface plot of wear rate vs. specific wear rate vs. temperature increase and (**d**) surface plot of friction coefficient vs. specific wear rate vs. temperature increase.

3.7. Analysis of Interaction Plots

The interaction graphs (Figures 11–14) indicate the combined effects of nanoclay content, load, sliding speed, and sliding distance on wear rate, friction coefficient, specific wear rate, and temperature increase. These figures demonstrate how each element affects the responses when altered simultaneously, offering insights into the intricate interactions in PVDF/nanoclay composites.

Figure 11 shows an interaction plot for the wear rate. The wear rate is greatly controlled by interactions between load and nanoclay content. Higher loads increase the wear rate, especially in composites lacking nanoclay, but adding nanoclay typically lowers wear across all situations. The influence of the sliding distance and load is also evident, with longer distances leading to more wear, particularly under increased load. The effect of sliding speed is quite small in contrast, exhibiting little influence on the wear rate when interacting with other parameters.

Figure 12 shows an interaction plot for the friction coefficient, which demonstrates a substantial correlation between nanoclay content and load. As load increases, friction also rises, particularly in samples without nanoclay. The use of nanoclay efficiently decreases friction at all load levels. Interactions between sliding speed and sliding distance follow a similar pattern, with greater speeds and lengths somewhat increasing friction, though the impact is less noticeable than that of load. This figure emphasizes the function of nanoclay in decreasing friction, particularly under greater load situations.

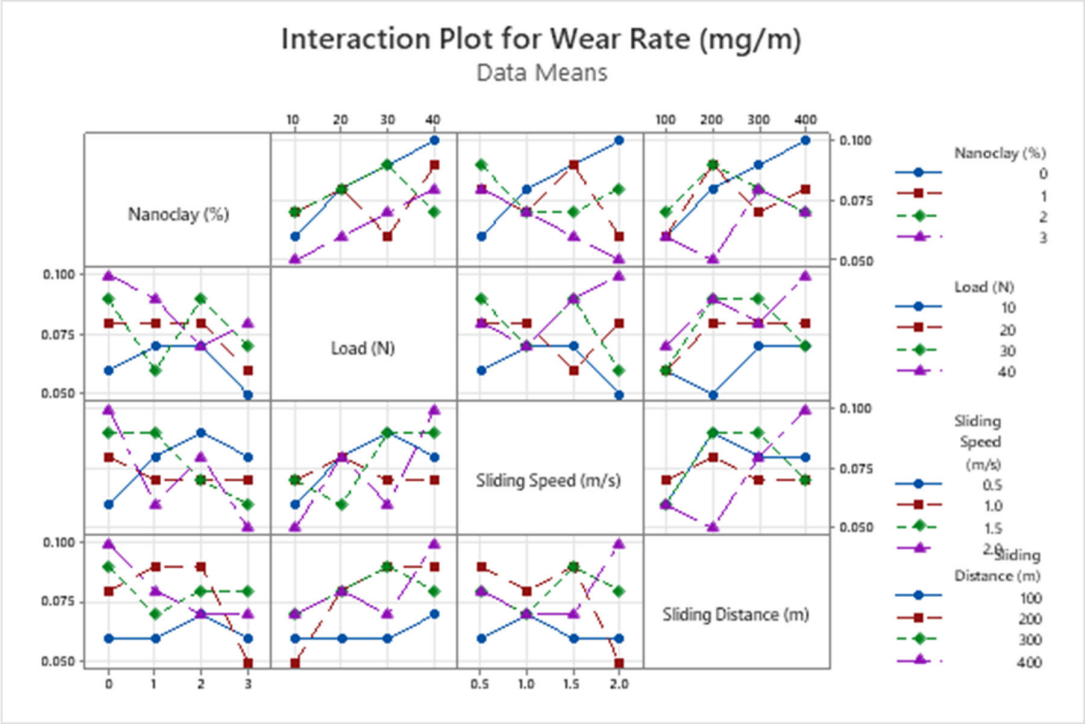


Figure 11. Interaction plot for wear rate.

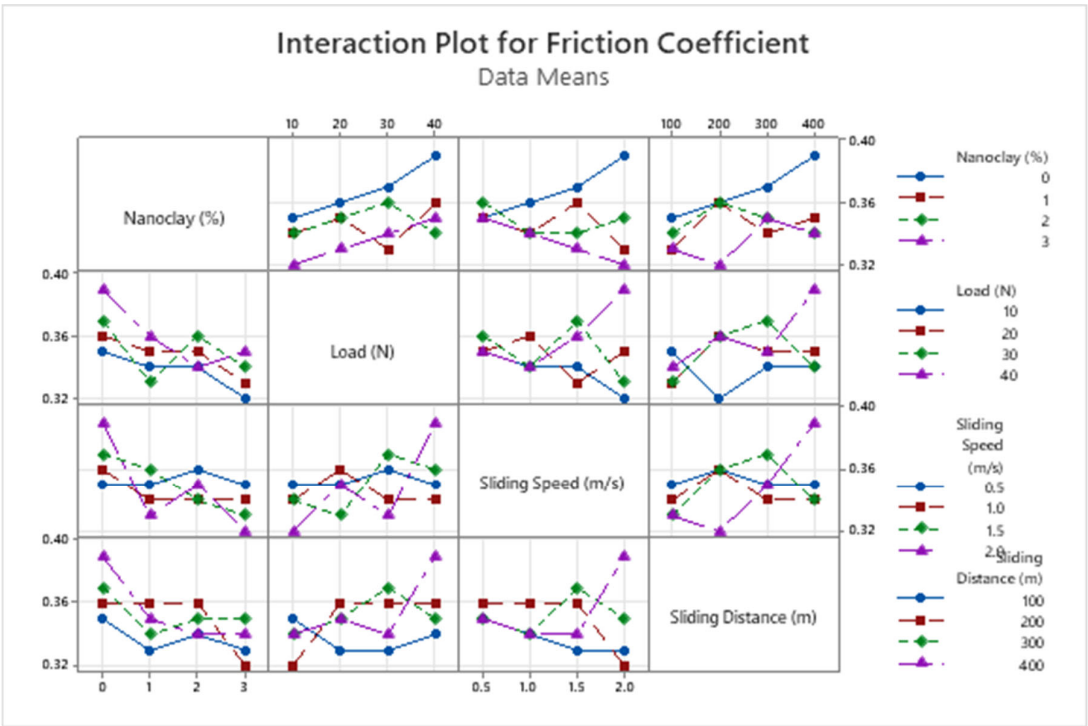


Figure 12. Interaction plot for friction coefficient.

Figure 13 portrays an interaction plot for the specific wear rate, which is greatly impacted by load and sliding distance. The specific wear rate increases with both parameters, particularly for high-load and long-distance combinations. Nanoclay content interacts favorably by lowering the specific wear rate, especially at lower loads, showing that nanoclay helps distribute wear more uniformly under less-severe circumstances. The influence of

sliding speed is generally low but reveals that higher speeds marginally increase particular wear rates when paired with high load and distance.

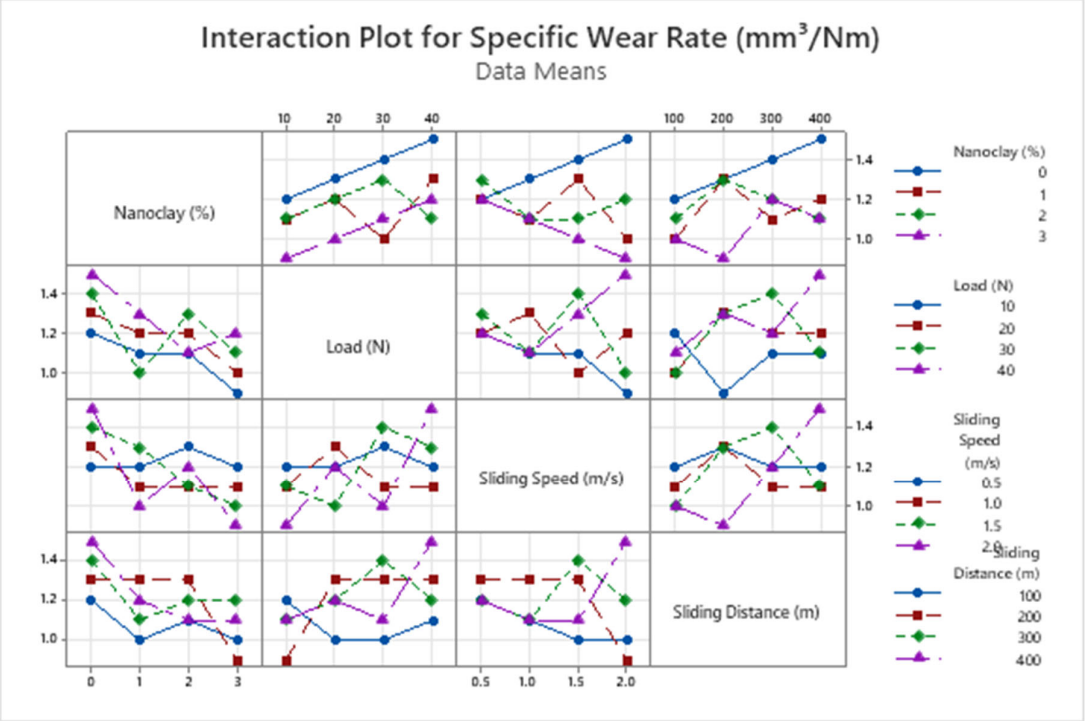


Figure 13. Interaction plot for specific wear rate.

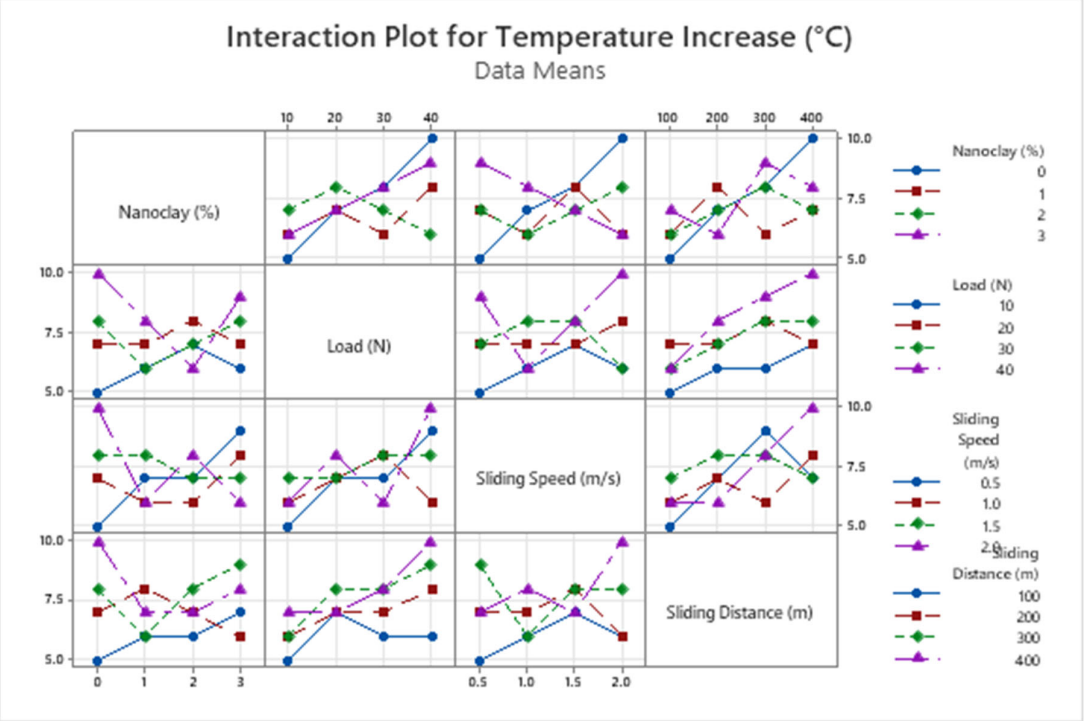


Figure 14. Interaction plot for temperature increase.

Figure 14 shows an interaction plot for temperature increase, which is mostly caused by interactions between load and sliding distance. Higher loads and longer distances result in considerable temperature increases due to higher frictional heating. Nanoclay content has a modest influence on temperature growth, demonstrating that nanoclay's role

is essentially mechanical rather than thermal. The sliding speed also adds moderately to the temperature rise when associated with high load, as predicted by higher frictional forces.

3.8. Comparative Analysis

The statistics in Table 10 make it clear that the tribological properties of PVDF/nanoclay composites are superior to those of other polymer composites reinforced with CNTs, graphene, nanoclay, glass fibers and TiO_2 nanoparticles. In particular, this study reported the wear rate and specific wear rate ranging from 0.05 0.1 mg/m and 0.9 1.5 mm^3/Nm, respectively, which had previously been considered some of the best results in this domain, indicating the possibility of utilizing nanoclay as an effective addition for wear resistance.

Table 10. General linear model: specific wear rate (mm^3/Nm) versus nanoclay (wt.%), load (N), sliding speed (m/s), sliding distance (m).

Study	Polymer Matrix	Reinforcement	Load (N)	Speed (m/s)	Distance (m)	Wear Rate (mg/m)	Specific Wear Rate (mm^3/Nm)	CoF	Thermal Stability	Tribological Insights
This Study	PVDF	Nanoclay (0–3 wt.%)	10–40	0.5–2.0	100–400	0.05–0.1	0.9–1.5	0.32–0.39	Significant	Enhanced β-phase crystallization; optimal wear and CoF at 3 wt.% nanoclay.
[45]	PP	Nanoclay (1–5 wt.%)	10–30	0.5–1.5	100–300	0.06–0.12	1.1–1.6	0.35–0.41	Moderate	Wear resistance improved up to 3 wt.% nanoclay but less effective at higher loads.
[46]	PVDF	CNTs (0–5 wt.%)	5–20	0.3–1.0	50–200	0.07–0.11	1.0–1.4	0.33–0.40	Low	Agglomeration of CNTs increased CoF despite improved wear resistance.
[47]	HDPE	Nanoclay (0–5 wt.%)	10–50	1.0–3.0	100–500	0.08–0.15	1.2–1.8	0.36–0.42	Low	Higher CoF observed at higher nanoclay concentrations.
[48]	PVDF	Graphene (0–2 wt.%)	15–25	0.5–2.0	100–300	0.06–0.09	0.8–1.2	0.31–0.37	Moderate	Enhanced wear resistance without significant β-phase induction.
[49]	Nylon	Glass Fibers (0–10 wt.%)	10–40	1.0–2.0	100–300	0.10–0.20	1.5–2.0	0.40–0.45	High	Glass fibers improved thermal stability but had limited wear reduction.
[50]	PVDF	TiO_2 (0–3 wt.%)	5–20	0.3–1.0	50–200	0.07–0.10	0.9–1.3	0.33–0.38	High	Improved wear resistance and thermal stability, less effective under high load.

Nanoclay, on the other hand, offers this possibility by suppressing agglomeration, though it enhances the β-phase crystallization process, which was unique to the study. Also, the CoF of PVDF/nanoclay composites was lower (0.32–0.39) than that of HDPE and nylon-based composites, indicating better performance in frictional constancy. In this respect, the findings further emphasize the enhanced thermal performance coefficients of

PVDF/nanoclay composites that make them candidates for high-performance applications in the aerospace, automotive and biomedical industries.

Such a comparison proves that nanoclay does exert a reinforcing effect and confirms the promise of PVDF/nanoclay composites for applications where low friction and high thermal stability, alongside high wear resistance, are needed.

4. Conclusions

This work comprehensively studied the tribological characteristics of PVDF/nanoclay composites and investigated the effects of nanoclay content, load, sliding speed, and sliding distance on the wear rate, friction coefficient, specific wear rate, and temperature. Using the Taguchi Design of Experiments technique, the major findings emphasized the measurable benefits of nanoclay reinforcement and provided insights into the relationships between the evaluated components. The results indicated that the nanoclay content considerably lowered the wear and friction in the PVDF composites. A nanoclay concentration of 3 wt.% produced the lowest wear rate at 0.05 mg/m under a load of 10 N and sliding distance of 100 m. Across all test circumstances, the use of nanoclay decreased wear rates by roughly 23% compared to unreinforced PVDF, demonstrating its efficiency in mitigating material loss through enhanced hardness and load distribution.

The load and sliding distance appeared as important parameters impacting the wear performance, with the greatest wear rate reported at 0.10 mg/m under a load of 40 N and a sliding distance of 400 m. This wear rate was approximately twice that of the lowest recorded wear rate, demonstrating the significant impact of the load on the driving material loss. A friction coefficient study also found that large loads increase friction, reaching a peak of 0.38 at 40 N. However, with 3 wt.% nanoclay, the friction coefficient was consistently lowered by approximately 12%, increasing the composite's resilience under high-stress conditions. Interaction plots and ANOVA findings were used to further evaluate the impact of coupled variables. Nanoclay content provided 51.29% of the decrease in the particular wear rate, whereas the load and sliding distance decreased by 22.47% and 16.98%, respectively. Additionally, the temperature increase due to frictional heating was maximum (10 °C) for a load of 40 N and a sliding distance of 400 m. Nanoclay addition decreased this temperature increase, with composites demonstrating a 15% lower temperature rise on average compared to unreinforced PVDF.

Material characterization using XRD and FTIR revealed the effective incorporation of nanoclay within the PVDF matrix, whereas SEM examination visibly supported the decrease in surface wear. The SEM images indicated smoother surfaces in the nanoclay-reinforced materials, with less-severe wear tracks and debris deposition, especially under high-load conditions. In summary, this work illustrates the major gains in wear resistance, friction reduction, and thermal stability of PVDF/nanoclay composites, with nanoclay content being important for increasing performance. These results imply that PVDF composites with 3 wt.% nanoclay are best for applications requiring strong wear resistance. Future studies should focus on sophisticated modeling tools, such as molecular dynamics simulations, to provide deeper insights into molecular interactions and confirm the findings over broader operating circumstances.

Author Contributions: Supervision, visualization, validation, and writing—original draft preparation were performed by P.H.; formal analysis, resources, and writing—review and editing by R.C.S.; conceptualization, resources, and writing—review and editing by G.B.K.; investigation, software, and formal analysis by N.N. All authors have read and agreed to the published version of the manuscript.

Funding: This study received no external funding.

Data Availability Statement: The data supporting the findings of this study are included within this article. All relevant experimental details, analysis, and results are presented in the manuscript and its accompanying figures and tables.

Conflicts of Interest: The authors declare no conflicts of interest.

List of Abbreviations

PVDF	Polyvinylidene Fluoride
PMMA	Polymethyl Methacrylate
XRD	X-Ray Diffraction
FTIR	Fourier Transform Infrared Spectroscopy
SEM	Scanning Electron Microscopy
DMF	Dimethyl Formamide
DOE	Design of Experiments
ANOVA	Analysis of Variance
S/N	Signal-to-Noise Ratio
ASTM	American Society for Testing and Materials

References

1. Vorkapić, M.; Bajić, D.M.; Baltić, M.; Nešić, D.; Mladenović, I. Mechanical properties of laminate materials based on polylactic acid and polyvinyl chloride meshes as reinforcement. *Tribol. Mater.* **2024**, *3*, 35–43. [CrossRef]
2. Sui, Y.; Cui, Y.; Meng, X.; Zhou, Q. Research progress on the correlation between properties of nanoparticles and their dispersion states in polymer matrix. *J. Appl. Polym. Sci.* **2022**, *139*, 52096. [CrossRef]
3. Weber, F.; Dötschel, V.; Steinmann, P.; Pfaller, S.; Ries, M. Evaluating the impact of filler size and filler content on the stiffness, strength, and toughness of polymer nanocomposites using coarse-grained molecular dynamics. *Eng. Fract. Mech.* **2024**, *307*, 110270. [CrossRef]
4. Zhang, X.; Li, B.; Dong, L.; Liu, H.; Chen, W.; Shen, Y.; Nan, C. Superior Energy Storage Performances of Polymer Nanocomposites via Modification of Filler/Polymer Interfaces. *Adv. Mater. Interfaces* **2018**, *5*, 1800096. [CrossRef]
5. Qian, M.; Zou, B.; Chen, Z.; Huang, W.; Wang, X.; Tang, B.; Liu, Q.; Zhu, Y. The Influence of Filler Size and Crosslinking Degree of Polymers on Mullins Effect in Filled NR/BR Composites. *Polymers* **2021**, *13*, 2284. [CrossRef]
6. Suthar, V.; Joseph, J.; Kadam, S.; Bhatt, R.; Shah, B. Functionalized polymer nanocomposites for dielectric applications. In *Advances in Functionalized Polymer Nanocomposites*; Elsevier: Amsterdam, The Netherlands, 2024; pp. 915–958.
7. Bai, Y.; Liu, Y.; Lv, H.; Shi, H.; Zhou, W.; Liu, Y.; Yu, D.-G. Processes of Electrospun Polyvinylidene Fluoride-Based Nanofibers, Their Piezoelectric Properties, and Several Fantastic Applications. *Polymers* **2022**, *14*, 4311. [CrossRef]
8. Wang, H.-Q.; Wang, J.-W.; Wang, X.-Z.; Gao, X.-H.; Zhuang, G.-C.; Yang, J.-B.; Ren, H. Dielectric properties and energy storage performance of PVDF-based composites with MoS_2@MXene nanofiller. *Chem. Eng. J.* **2022**, *437*, 135431. [CrossRef]
9. Jing, L.; Li, W.; Gao, C.; Li, M.; Fei, W. Excellent energy storage properties achieved in PVDF-based composites by designing the lamellar-structured fillers. *Compos. Sci. Technol.* **2022**, *227*, 109568. [CrossRef]
10. Bismarck, A.; Schulz, E. Adhesion and friction behavior between fluorinated carbon fibers and poly(vinylidene fluoride). *J. Mater. Sci.* **2003**, *38*, 4965–4972. [CrossRef]
11. Li, N.; Lu, Q.; Yin, W.; Xiao, C.; Li, J. The structure and properties of poly(vinylidene fluoride)/ultrahigh-molecular-weight polyethylene blend hollow fiber membranes via TIPS with mixed diluents. *J. Membr. Sci.* **2020**, *595*, 117527. [CrossRef]
12. Afonso, E.; Martínez-Gómez, A.; Tiemblo, P.; García, N. Exploring chemical and structural features to tailor wetting properties of PVDF and PVDF/PMMA surfaces. *Polymer* **2022**, *262*, 125441. [CrossRef]
13. Hintermueller, D.; Prakash, R. Comprehensive Characterization of Solution-Cast Pristine and Reduced Graphene Oxide Composite Polyvinylidene Fluoride Films for Sensory Applications. *Polymers* **2022**, *14*, 2546. [CrossRef] [PubMed]
14. Paul, A.; Kesharvani, S.; Agrawal, A.; Dwivedi, G.; Singh, V.; Saxena, K.K. Mechanical and tribological properties of nano clay/PMMA composites extruded with a twin-screw extruder. *Proc. Inst. Mech. Eng. Part E J. Process Mech. Eng.* **2023**, 09544089231215224. [CrossRef]
15. Thangavel, E.; Ramasundaram, S.; Pitchaimuthu, S.; Hong, S.W.; Lee, S.Y.; Yoo, S.-S.; Kim, D.-E.; Ito, E.; Kang, Y.S. Structural and tribological characteristics of poly(vinylidene fluoride)/functionalized graphene oxide nanocomposite thin films. *Compos. Sci. Technol.* **2014**, *90*, 187–192. [CrossRef]
16. Abu-Zurayk, R.; Alnairat, N.; Bozeya, A.; Khalaf, A.; Abu-Dalo, D. Enhanced properties of PVDF membranes using green Ag-nanoclay composite nanoarchitectonics. *Mater. Res. Express* **2024**, *11*, 045007. [CrossRef]

17. Hosseini, S.M.; Yousefi, A.A. Electrospun PVDF/MWCNT/OMMT hybrid nanocomposites: Preparation and characterization. *Iran. Polym. J.* **2017**, *26*, 331–339. [CrossRef]
18. Saralch, S.; Jagota, V.; Pathak, D.; Singh, V. Response surface methodology based analysis of the impact of nanoclay addition on the wear resistance of polypropylene. *Eur. Phys. J. Appl. Phys.* **2019**, *86*, 10401. [CrossRef]
19. Gaur, A.; Rana, D.; Maiti, P. Mechanical and wear behaviour of poly(vinylidene fluoride)/clay nanocomposite. *J. Mater. Res. Technol.* **2019**, *8*, 5874–5881. [CrossRef]
20. Alami, M.; Mokaddem, A.; Belkheir, M.; Rouissat, M.; Doumi, B.; Ziani, D. Improving the performance of hybrid biocomposite materials using epoxy, vinyl ester and polyimide polymer matrix: Comparative study. *Appl. Eng. Lett. J. Eng. Appl. Sci.* **2024**, *9*, 64–75. [CrossRef]
21. Marković, A.; Ivanović, L.; Stojanović, B. Characteristics, Manufacturing, and Testing Methods of Polymer Gears: Review. In Proceedings of the International Conference on Organization and Technology of Maintenance, Osijek, Croatia, 12 December 2023; Springer Nature: Cham, Switzerland, 2024; pp. 269–282.
22. Hiremath, P.; Ranjan, R.; DeSouza, V.; Bhat, R.; Patil, S.; Maddodi, B.; Shivamurthy, B.; Perez, T.C.; Naik, N. Enhanced Wear Resistance in Carbon Nanotube-Filled Bio-Epoxy Composites: A Comprehensive Analysis via Scanning Electron Microscopy and Atomic Force Microscopy. *J. Compos. Sci.* **2023**, *7*, 478. [CrossRef]
23. Zhang, L.-Q.; Yang, S.-G.; Zhang, J.-H.; Zhong, K.-P.; Zhao, Z.-G.; Chen, Y.-H.; Lei, J.; Zhang, Q.-Y.; Li, Z.-M. Insight into the Excellent Tribological Performance of Highly Oriented Poly(phenylene sulfide). *Chin. J. Polym. Sci.* **2022**, *40*, 290–298. [CrossRef]
24. Häggström, D.; Sellgren, U.; Björklund, S. Thermomechanical performance of carbon fiber reinforced polymer synchronizer friction liners. *Proc. Inst. Mech. Eng. Part J J. Eng. Tribol.* **2022**, *236*, 1074–1080. [CrossRef]
25. Essifi, K.; Hammani, A.; Berraaouan, D.; El Bachiri, A.; Fauconnier, M.-L.; Tahani, A. Montmorillonite nanoclay based formulation for controlled and selective release of volatile essential oil compounds. *Mater. Chem. Phys.* **2022**, *277*, 125569. [CrossRef]
26. Behroozi, M.; Pakizeh, M. Study the effects of Cloisite15 A nanoclay incorporation on the morphology and gas permeation properties of Pebax2533 polymer. *J. Appl. Polym. Sci.* **2017**, *134*, 45302. [CrossRef]
27. Vishal, K.; Rajkumar, K. Dry sliding wear behavior of Poly Ether Ether Ketone (PEEK) reinforced with graphite and synthetic diamond particles. *Diam. Relat. Mater.* **2022**, *130*, 109404. [CrossRef]
28. Malayoglu, U. Removal of heavy metals by biopolymer (chitosan)/nanoclay composites. *Sep. Sci. Technol.* **2018**, *53*, 2741–2749. [CrossRef]
29. Biglari Quchan Atigh, Z.; Heidari, A.; Karimi, A.; Pezhman, M.A.; Lajayer, B.A.; Lima, E.C. Purification and economic analysis of nanoclay from bentonite. *Environ. Sci. Pollut. Res.* **2021**, *28*, 13690–13696. [CrossRef]
30. Manafi, S.; Kiahosseini, S.R. Polytetrafluoroethylene/nanoclay composite as anti-wearing compound. *Iran. Polym. J.* **2020**, *29*, 25–35. [CrossRef]
31. Tripathi, V.K.; Ambekar, S. Optimization and Analysis of Wear Rate of CFRP-NanoZno/Nanoclay Hybrid Composites Using RSM. *J. Bio-Tribo-Corros.* **2019**, *5*, 96. [CrossRef]
32. Nazari, A. An experimental investigation on the flexural and wear properties of multiscale nanoclay/basalt fiber/epoxy composites. *Polym. Compos.* **2021**, *42*, 5755–5762. [CrossRef]
33. Saha, D.; Satapathy, B.K. Tuning of Friction Oscillation Amplitude in Halloysite, Montmorillonite, and Wollastonite Filled Friction Composites: Load, Speed, and Temperature Sensitivity. *J. Tribol.* **2022**, *144*, 061706. [CrossRef]
34. Namdev, A.; Purohit, R.; Telang, A.; Kumar, A.; Saxena, K.K.; Mabuwa, S.; Msomi, V.; Mohammed, K.A. Optimization of dry sliding wear behavior of epoxy nanocomposites under different conditions. *Mater. Res. Express* **2022**, *9*, 065303. [CrossRef]
35. Talib, A.A.A.; Jumahat, A.; Jawaid, M.; Sapiai, N.; Nagarajan, R. Wear properties of nanoclay modified basalt fibre composites under dry adhesive sliding, two-body abrasive, and slurry pot erosive. *Polym. Bull.* **2022**, *79*, 10823–10840. [CrossRef]
36. Vishal, K.; Rajkumar, K.; Annamalai, V.E. Wear and tribofilm characterization of bamboo CNT (B-CNT)-peek composite with incremental blending of submicron synthetic diamond particles. *Wear* **2021**, *466–467*, 203556. [CrossRef]
37. Kowshik, S.; Rao, U.S.; Sharma, S.; Hiremath, P.; Prasad, K.S.R.; Naik, N.; Bhat, R.; Kasipandian, K. Mechanical Properties of Eggshell Filled Non-Post-Cured and Post-Cured GFRP Composites: A Comparative Study. *ES Mater. Manuf.* **2023**, *22*, 1043. [CrossRef]
38. Zade, S.K.; Babu, V.S.; Srinadh, K.S. Effect of nanoclay, glass fiber volume and orientation on tensile strength of epoxy-glass composite and optimization using Taguchi method. *World J. Eng.* **2018**, *15*, 312–320. [CrossRef]
39. Singh, T.; Patnaik, A.; Chauhan, R.; Chauhan, P.; Kumar, N. Physico-mechanical and tribological properties of nanoclay filled friction composite materials using Taguchi design of experiment approach. *Polym. Compos.* **2018**, *39*, 1575–1581. [CrossRef]
40. Hiremath, P.; Kini, U.A.; Shettar, M.; Sharma, S.; Jayashree, P.K. Investigation on tensile properties and analysis of wear property of glass fiber-epoxy-nanoclay ternary nanocomposite using response surface methodology. *Cogent Eng.* **2021**, *8*, 1877869. [CrossRef]
41. Kiran, Z.S.; Babu, V.; Srinadh, K. Investigation of the microhardness and solid particle erosive wear of organoclay-filled glass-epoxy nanocomposites and optimisation using Taguchi method. *Aust. J. Mech. Eng.* **2020**, *18*, 364–374. [CrossRef]

42. Jagadeesh, P.; Rangappa, S.M.; Siengchin, S. Tribological performance analysis of sustainable basalt micro-filler loaded bio-based polypropylene and high density polyethylene composites. *J. Thermoplast. Compos. Mater.* **2024**, *37*, 3252–3293. [CrossRef]
43. Mahesh, G.G.; Kandasamy, J. Experimental investigations on the drilling parameters to minimize delamination and taperness of hybrid GFRP/Al_2O_3 composites by using ANOVA approach. *World J. Eng.* **2023**, *20*, 376–386. [CrossRef]
44. Srivastava, P.; Singh, V.P. Optimizing tribological performance of 3D-printed poly(lactic acid) components through process parameter analysis. *Iran. Polym. J.* **2024**, 1–18. [CrossRef]
45. Faraj, R.H.; Mohammed, A.A.; Omer, K.M. Self-compacting concrete composites modified with nanoparticles: A comprehensive review, analysis and modeling. *J. Build. Eng.* **2022**, *50*, 104170. [CrossRef]
46. Sanaeepur, H.; Amooghin, A.E.; Shirazi, M.M.A.; Pishnamazi, M.; Shirazian, S. Water desalination and ion removal using mixed matrix electrospun nanofibrous membranes: A critical review. *Desalination* **2022**, *521*, 115350. [CrossRef]
47. Qaidi, S.; Yahia, A.; Tayeh, B.A.; Unis, H.; Faraj, R.; Mohammed, A. 3D printed geopolymer composites: A review. *Mater. Today Sustain.* **2022**, *20*, 100240. [CrossRef]
48. Zhao, B.; Hamidinejad, M.; Wang, S.; Bai, P.; Che, R.; Zhang, R.; Park, C.B. Advances in electromagnetic shielding properties of composite foams. *J. Mater. Chem. A* **2021**, *9*, 8896–8949. [CrossRef]
49. Panin, S.V.; Alexenko, V.O.; Buslovich, D.G. High Performance Polymer Composites: A Role of Transfer Films in Ensuring Tribological Properties—A Review. *Polymers* **2022**, *14*, 975. [CrossRef]
50. Manteghi, M.; Kumar, S.; Early, J.; Adusumalli, B. *High Performance Commercial Fenestration Framing Systems*; National Energy Technology Laboratory: Pittsburgh, PA, USA; Morgantown, WV, USA, 2010. [CrossRef]

Disclaimer/Publisher's Note: The statements, opinions and data contained in all publications are solely those of the individual author(s) and contributor(s) and not of MDPI and/or the editor(s). MDPI and/or the editor(s) disclaim responsibility for any injury to people or property resulting from any ideas, methods, instructions or products referred to in the content.